https://doi.org/10.5194/egusphere-2026-3384
Preprint. Discussion started: 6 July 2026

Unravelling the source for diverging long-term ice loss trajectories within the Greenland Ice sheet Coupled Model Intercomparison Project (GrICMIP)

Clemens Schannwell[1], Marie-Luise Kapsch[1], Matteo Willeit[2], Lars Ackermann[3], Gregor Knorr[3], Uta Krebs-Kanzow[3], Gerrit Lohmann[3,4], Katharina D. Six[1], Christian Stepanek[3], and Uwe Mikolajewicz[1]

[1]Max Planck Institute for Meteorology, Hamburg, Germany
[2]Potsdam Institute for Climate Impact Research, Member of the Leibniz Association, Potsdam, Germany
[3]Alfred Wegener Institute, Helmholtz Center for Polar and Marine Research, Bremerhaven, Germany
[4]IUP and MARUM, University of Bremen, Bremen, Germany

Correspondence: Clemens Schannwell (clemens.schannwell@mpimet.mpg.de)

Abstract. The long-term evolution of the Greenland Ice Sheet (GrIS) remains a major source of uncertainty in projections of future sea-level rise. Recent advances in coupled climate–ice sheet models provide new opportunities to investigate the role of feedbacks between the ice sheet and the climate system, yet substantial divergence persists across climate-ice sheet model projections. Here, we present results from the Greenland Ice sheet Coupled Model Intercomparison Project (GrICMIP), using three coupled climate–ice sheet models to simulate GrIS evolution under multiple emission scenarios to the year 4000 CE. While projected sea-level contributions remain modest by 2100 (0.03–0.11 m), they diverge strongly on longer timescales, reaching up to 3.5 m by 2500. Under the high-emission scenario, full GrIS disintegration is projected as early as 3000 CE. By means of targeted sensitivity experiments, we identify the dominant sources of diverging GrIS trajectories. Across all models, changes in surface mass balance (SMB), and in particular net surface melt, control the long-term ice-sheet retreat. Differences in SMB formulation, especially in the underlying energy balance models, together with differences in the simulated climate, outweigh the influence of initial ice-sheet geometry. This establishes a hierarchy of uncertainties in which atmospheric processes and their representation within the model systems propagate non-linearly into ice-sheet evolution. Our results demonstrate that reliable long-term projections of the GrIS critically depend on improving the representation of climate and SMB, rather than on refining initial conditions alone.

1 Introduction

Rising global sea level, with substantial contributions from mass loss of the major ice sheets in Greenland and Antarctica, poses a challenge with far-reaching socio-economic consequences (Kirezci et al., 2020; Depsky et al., 2023). Since 1990, the overall mass loss of the Greenland ice sheet (GrIS) has changed from a near zero contribution to ∼250 Gt/yr or ∼0.7 mm/yr sea-level equivalent (SLE) in the 2010s (Mankoff et al., 2021). This accelerating ice mass loss trend is likely to continue over the coming decades and centuries, with high-end sea-level rise projections from the GrIS reaching beyond 3 m SLE by 2300 (Goelzer et al., 2025). While ice-ocean interactions and ice dynamics play a non-negligible role for the GrIS mass balance on

https://doi.org/10.5194/egusphere-2026-3384
Preprint. Discussion started: 6 July 2026

decadal timescales, the dominant driver for future mass loss of the GrIS is expected to be a changing surface mass balance (SMB, Fürst et al., 2015; Aschwanden et al., 2019; Goelzer et al., 2020). Since changes in the SMB are tightly linked to changes in near-surface air temperature, the importance of the SMB is even enhanced for higher emission scenarios and longer centennial to millennial timescales. In such scenarios, the margins of the GrIS retreat rapidly, reducing the contact area between the ice and the ocean, and turning the GrIS effectively into a land-terminating ice sheet (Fürst et al., 2015).

Typically, GrIS projections have been performed with stand-alone ice-sheet models (e.g. Fürst et al., 2015; Calov et al., 2018; Aschwanden et al., 2019; Goelzer et al., 2020; Rahlves et al., 2025) that largely omit feedbacks between the climate and ice sheets. The recent emergence of coupled climate-ice sheet models now allows to explore the importance of climate-ice sheet feedbacks for the future evolution of the GrIS. However, their high computational costs has restricted the application horizon of coupled climate-ice sheet models almost exclusively to timescales of up to year 2300, with a strong focus on high-end emission scenarios (e.g. Mikolajewicz et al., 2007b; Vizcaino et al., 2015; Muntjewerf et al., 2020; Madsen et al., 2022). Because of the long response time of ice sheets relative to other components of the climate system, such as the atmosphere or the ocean, the 300 year timescale is insufficient to deduce the importance of climate-ice sheet interactions on the global climate as well as the ice-sheet evolution (Vizcaino et al., 2015; Haubner et al., 2026). To date, coupled projections on millennial timescales have been limited to regional model configurations (Paice et al., 2026). As the field of climate-ice sheet modelling is still in its infancy, explanations for the substantial differences in the future evolution of the GrIS using such coupled models have not been explored. For example, Madsen et al. (2022) and Muntjewerf et al. (2020) performed the same forcing experiment with EC-Earth-PISM and CESM2.1-CISM2.1, respectively. Both models start off the forcing experiment with an almost identical integrated SMB. However, at the end of their 300-year long simulations, the SMBs vary by a factor of four.

Here, we build upon these findings and present the results of the Greenland Ice sheet Coupled Model Intercomparison Project (GrICMIP). We use three different coupled climate-ice sheet models, specifically tailored towards millennial timescales, to investigate the future response of the GrIS to different emission scenarios. We go beyond previous studies by exploring the climate evolution until year 4000 CE. In addition, we perform targeted sensitivity simulations that allow us to disentangle the driving mechanisms behind changes in the SMB across the different models. The paper is structured as follows: In the methods section, we introduce each of the three climate-ice sheet models and underlying energy balance models (EBMs) used to calculate the SMB and provide a detailed description of the performed experiments. The results section bridges the gap between global and regional scales, starting with the global climate evolution before zooming into Greenland, and then illuminates the drivers behind differences in the simulated SMB. The paper closes with a discussion and conclusion.

2 Methods

For our analysis, we use two comprehensive Earth System Models (ESMs) and one Earth System Model of Intermediate Complexity (EMIC), which all include an interactive GrIS. All three models are designed for millennial-scale simulations. This comes at the expense of spatial resolution, preventing the explicit representation of small-scale climatic processes, such as

https://doi.org/10.5194/egusphere-2026-3384
Preprint. Discussion started: 6 July 2026

katabatic winds. Each model system uses a different approach to calculate the SMB. In the following, we provide a description of each coupled model system and highlight differences between them.

2.1 Model description

The models differ in their atmosphere, land and ocean components as well as in additional modules that are used to simulate changes in the bathymetry, land-sea mask and/or icebergs. All climate-ice sheet models or their sub-components have widely been used for paleo and future applications (Ackermann et al., 2020; Mikolajewicz et al., 2025; Niu et al., 2024, 2025; Willeit et al., 2024) and participated in a variety of model intercomparisons (Fettweis et al., 2020; Kageyama et al., 2021; Renoult et al., 2020). The most relevant information on the model systems in terms of their individual components is given in Table 1. Additional parameter values for the ice sheet and solid Earth models are listed in Table A1. Details on the utilized EBMs are described in Section 2.1.4.

2.1.1 CLIMBER-X

We use the fast Earth system model CLIMBER-X (Willeit et al., 2022, 2023, 2024) with the ice-sheet model SICOPOLIS (Greve, 1997) applied to the GrIS domain. CLIMBER-X includes the frictional-geostrophic 3D ocean model GOLDSTEIN (Edwards et al., 1998; Edwards and Marsh, 2005), the semi-empirical statistical-dynamical atmosphere model SESAM (Willeit et al., 2022), the dynamic-thermodynamic sea-ice model SISIM (Willeit et al., 2022), the land-surface model with interactive vegetation PALADYN (Willeit and Ganopolski, 2016) and the ocean biogeochemistry model HAMOCC6 (Ilyina et al., 2013; Mauritsen et al., 2019). The comprehensive carbon cycle in the model computes the atmospheric CO_2 and CH_4 evolution interactively, while accounting for slow processes associated with permafrost, marine sediments and chemical rock weathering, which are important on millennial time scales. All components of the climate model have a horizontal resolution of $5° \times 5°$. The dynamics of the GrIS in SICOPOLIS is represented at a horizontal resolution of 16 km, coupled to the climate model via the physically-based surface energy and mass balance interface SEMIX (Willeit et al., 2024) with a coupling time step of one year. We employ a parametrisation of sub-grid ice discharge into the ocean from unresolved narrow outlet glaciers dynamics (Calov et al., 2015). The basal melt of floating ice shelves is computed from simulated ocean temperature and salinity (Willeit et al., 2024). The viscoelastic solid Earth model VILMA (Klemann et al., 2008; Martinec et al., 2018; Bagge et al., 2021) computes the glacial isostatic adjustment and relative sea-level changes. Simulated changes in the ice sheet have an impact on climate through changes in elevation, surface albedo, river directions, meltwater and calving fluxes into the ocean, and land-sea mask (Willeit et al., 2024). The climate model is described in detail in Willeit et al. (2022), the carbon cycle model in Willeit et al. (2023) and the ice-sheet coupling in Willeit et al. (2024). The Antarctic ice sheet is held constant and prescribed from present-day observations. In the following, the coupled climate-ice sheet model is referred to as CLIMBER-X.

https://doi.org/10.5194/egusphere-2026-3384
Preprint. Discussion started: 6 July 2026

2.1.2 AWI-ESM

We further use the Alfred Wegener Institute Earth System Model version 2 (AWI-ESM2) including the Parallel Ice Sheet Model (PISM) for the GrIS domain. The atmospheric component of AWI-ESM2 is the sixth generation of the European Centre for Medium-Range Weather Forecast Model Hamburg ECHAM6 (Stevens et al., 2013). It includes the dynamic vegetation model JSBACH (Reick et al., 2021) and a hydrological discharge model (Hagemann and Dümenil, 1997) that also accounts for changes in the land orography and river directions (Riddick et al., 2018) in response to ice sheet changes. The model resolution used is T63 (1.9°) in the horizontal domain with 47 vertical levels. The ocean component of AWI-ESM2, is the second version of the Finite volumE Sea ice-Ocean Model (Danilov et al., 2017, FESOM2,). The model uses an unstructured, multi-resolution grid with horizontal resolutions ranging from around 120 km in the subtropics to around 20 km in the high latitudes (Sein et al., 2016), with high resolution at critical regions, for example near coastlines. PISM 1.2.1 (Winkelmann et al., 2011; Martin et al., 2011) is used for the GrIS domain with a horizontal resolution of 5 km. The climate and ice sheet components run iteratively and are fully coupled with coupling time step of one year. The diurnal EBM (Krebs-Kanzow et al., 2021, dEBM,) is used with output from the atmosphere component ECHAM6 to provide the SMB for the ice sheet. The ice sheet further receives averaged ocean salinity and temperature fields at the ocean-ice sheet interface to compute basal melt underneath ice shelves. The coupling from the ice sheet to the climate components includes changes in orography, surface albedo, and freshwater fluxes due to changes in the total ice mass balance. The Antarctic ice sheet is prescribed and held fixed at its present-day geometry. Henceforth, the coupled climate-ice sheet setup is referred to as AWI-ESM.

2.1.3 MPI-ESM

We additionally use the Max Planck Institute for Meteorology Earth System Model version 1.2 (MPI-ESM1.2) coupled to the modified Parallel Ice Sheet Model (mPISM) (Ziemen et al., 2019) and the solid Earth model VILMA (Klemann et al., 2008; Martinec et al., 2018). MPI-ESM1.2 uses the atmosphere general circulation model ECHAM6.3 (Stevens et al., 2013), including the dynamic vegetation model JSBACH (Raddatz et al., 2007). The atmosphere model resolution is T31 (approx. 3.75°) in the horizontal domain with 31 vertical levels. As global ocean component, MPIOM1.6 is applied (Marsland et al., 2003; Mikolajewicz et al., 2007a). The MPIOM setup used here has a resolution of 3° on an Arakawa C grid (Arakawa and Lamb, 1977), with grid poles over Greenland and Antarctica yielding a grid resolution between 391 km in the tropical Pacific and 31 km near Greenland. The MPIOM version applied here contains an Eulerian iceberg module (Erokhina and Mikolajewicz, 2024). Ice sheets are represented by the thermomechanically coupled ice-sheet model mPISM (Ziemen et al., 2019) based on PISM0.7.3. The polar stereographic grid has a resolution of 10 km in the Northern Hemisphere and for Antarctica. Note, that for the current study, the Antarctic ice sheet is prescribed from a pre-industrial (PI) control simulation. The model system accounts for changes in the land orography and river directions (Riddick et al., 2018) and includes modules to change the land-sea mask and ocean bathymetry (Meccia and Mikolajewicz, 2018) due to changes in local sea level. To calculate the SMB, an EBM is used (Kapsch et al., 2021). Further, ocean salinity and temperature are extrapolated underneath ice shelves to calculate the basal melt rates. The model and its sub-components are described in detail in Mikolajewicz et al. (2025), although

https://doi.org/10.5194/egusphere-2026-3384
Preprint. Discussion started: 6 July 2026

the one utilized here differs in terms of its parameter settings, its resolution of the ice-sheet model for Antarctica, and its ocean grid. Details regarding these changes are described in Andernach et al. (2026). Here, a coupling time step of one year between MPI-ESM1.2 and mPISM/VILMA is used. The coupling scheme is sequential. In the following, we refer to the coupled model system as MPI-ESM.

2.1.4 SMB calculation

Here, we present the main characteristics of the EBMs that are applied within the three model systems to calculate surface melt, refreezing, and and accumulation. Although the EBMs substantially differ in their approach, they have all been tuned for historical climate conditions (see also Fettweis et al., 2020).

CLIMBER-X

CLIMBER-X uses the surface energy and mass balance interface SEMIX to compute the SMB of the ice sheet. SEMIX is largely based on the ideas in Calov et al. (2005), but with notable modifications and improvements. The climate model fields needed by SEMIX are first bilinearly interpolated from the coarse-resolution climate model grid (5°×5°) onto the high-resolution ice sheet model grid, where SEMIX operates. Subsequently, near-surface air temperature, humidity, and radiation fields are elevation corrected. For temperature a constant lapse rate of 5°C/km is used. There is no orographic correction in the precipitation downscaling. Snow albedo depends on snow grain size and the concentration of dust in snow, which is computed from the simulated dust deposition flux. The surface energy balance equation is then solved to compute surface melt and refreezing, and the SMB is finally derived accounting for snowfall, rainfall, sublimation and runoff. SEMIX is described in detail in Appendix B of Willeit et al. (2024).

AWI-ESM

AWI-ESM uses the diurnal EBM (dEBM, Krebs-Kanzow et al., 2021), which requires monthly means of longwave and shortwave radiation, near-surface air temperature, precipitation, and cloud cover. These climate fields are bilinearly interpolated from the coarse-resolution atmosphere grid onto the high-resolution ice sheet grid with a lapse-rate correction applied to the air temperature. For the near-surface air temperature a constant lapse rate of 5°C/km is used. No orographic correction is applied for the precipitation downscaling. The dEBM resolves sub-daily variability by partitioning monthly forcing fields into distinct clear-sky and cloudy-sky regimes, and, for clear-sky conditions, by separately computing daytime surface melt and nocturnal refreezing. The melt period is defined as the fraction of the diurnal cycle during which incoming shortwave radiation exceeds outgoing longwave radiation. This separation is derived analytically from the location- and time-dependent solar geometry based on orbital parameters. The melt period mean temperature is parameterised using the Positive degree days method (PDD, Calov and Greve, 2005). Different albedo values are assigned to new snow, dry snow, and wet snow, for both fair and cloudy conditions.

https://doi.org/10.5194/egusphere-2026-3384
Preprint. Discussion started: 6 July 2026

MPI-ESM

In MPI-ESM, the SMB is calculated by an EBM that calculates surface melt and accumulation rates from hourly atmospheric fields (Kapsch et al., 2021). The atmospheric fields are linearly interpolated onto elevation classes. To account for height differences between each elevation class and the surface elevation of the atmospheric model, a height correction is applied to near-surface air temperature, humidity, dew point temperature, precipitation, downward longwave radiation and near-surface density fields. Temperatures are corrected using a constant lapse rate of 4.7 Km^{-1}. Precipitation is corrected for elevations above 2000 m, taking into account the height desertification effect. Details on the applied height correction are described in Section 2.1.1 of Kapsch et al. (2021). To obtain surface melt rates, the EBM computes the energy balance at the atmosphere–snow interface as the sum over the radiative and turbulent as well as rain-induced and conductive heat fluxes. The albedo parameterisation in the EBM is based on the parameterisation by Oerlemans and Knap (1998) and considers snow ageing, snow depth and the influence of cloud coverage. The obtained 3-D fields of surface melt, accumulation and SMB are then vertically and horizontally interpolated onto the actual ice-sheet topography.

2.2 Experiments

To investigate the recent and future response of the GrIS to warming, we performed transient simulations with all three coupled climate-ice sheet models under historical (1850-2015) forcing and three different extended socio-economic pathways (SSPs) that extend almost 2000 years into the future (2016-4000). All three models started their simulations from a near-equilibrium state for PI. In addition, we conducted several sets of sensitivity simulations that allow us to disentangle the driving mechanisms behind changes in the SMB across the different models.

2.2.1 Projections

For the future projections, we applied all model systems under SSP2-4.5, SSP4-6.0 and SSP5-8.5 transient greenhouse gas forcing, branching off from historical experiments that range from 1850 to 2015 CE. As forcing, we utilized time-varying CO_2 and CH_4 levels from emission driven scenarios with CLIMBER-X. For details on the emission scenarios refer to Fig. 1 and the Supplementary Information of Kaufhold et al. (2025). The greenhouse gas N_2O is held constant at PI concentrations in all simulations. Solar insolation varies through changes in the Earth's orbital parameters, calculated following the algorithm of Berger and Loutre (1991) (MPI-ESM, AWI-ESM) and Laskar et al. (2004) (CLIMBER-X). The simulations are summarized in Table 1, along with other model-specific information. More details on the initialization methods can be found in Table A3. In the following, we discuss changes until year 2100, 2300, 2500, 3000 and 4000, which are defined as mean over the years 2071–2100, 2201–2300, 2401–2500, 2901–3000, and 3901–4000, respectively. The changes are calculated relative to the PI control period, here computed as mean over 1850–1949.

https://doi.org/10.5194/egusphere-2026-3384
Preprint. Discussion started: 6 July 2026

Model	Model resolution	Surface mass balance scheme	Climate sensitivity	Emission scenarios	Simulation years
CLIMBER-X	Atmosphere: 5° Ocean: 5° Ice sheet: 16 km	SEMIX (Willeit et al., 2024)	3.1°C	SSP2-4.5 SSP4-6.0 SSP5-8.5	1850–4000
AWI-ESM	Atmosphere: 1.9° Ocean: 20-120 km Ice sheet: 5 km	dEBM (Krebs-Kanzow et al., 2021)	3.1°C		
MPI-ESM	Atmosphere: 3.75° Ocean: 31-391 km Ice sheet: 10 km	EBM (Kapsch et al., 2021)	4.1°C		

Table 1. Simulation setup for the three model systems, including the resolution of individual model components, the energy balance model, the model's equilibrium climate sensitivity, the applied emission scenarios, as well as simulation lengths for the future projections. The equilibrium climate sensitivity is derived following the method by Gregory et al. (2004).

2.2.2 Sensitivity simulations

A variety of sensitivity experiments were performed to investigate the mechanisms driving differences in SMB between the model systems. We focus on three key contributions: (i) from the EBMs described in Section 2.1.4, (ii) the climate forcing produced by the respective climate models, and (iii) the underlying ice-sheet topography arising from differences in the climate and ice-sheet response between models (Table 2). The sensitivity experiments are performed with the different EBMs in a stand-alone mode. The simulations all cover the period from 2000–4000. For the analysis, we focus on the time slice 2100, because over this period climate and SMB changes relative to PI are already considerable, but changes in ice-sheet topography remain modest.

Energy Balance Model

To explore the influence of the choice of the EBM on the SMB, we have performed a set of simulations that utilize the same climate forcing and surface topography but differ in regards to the used EBM. For this, we used the atmospheric fields and the surface topography from the MPI-ESM simulations as forcing for each respective EBM. A comparison of these three experiments allows us to examine how much impact the different methods and parameterisations used in the EBMs have on the calculated SMB.

Climate forcing

To disentangle the effect of the atmospheric forcing on the SMB, we used the EBM of AWI-ESM. In these simulations, only the atmospheric forcing fields are interchanged between models while the EBM and the surface topography remains the one

https://doi.org/10.5194/egusphere-2026-3384
Preprint. Discussion started: 6 July 2026

of AWI-ESM. The forcing fields were downscaled from their original grid to the 5 km grid used for the Greenland domain in AWI-ESM (see section 2.1.4).

Ice-sheet topography

The impact of the simulated surface topography, which differs substantially between models, on the SMB has been investigated by three additional simulations. For this, we used the atmospheric fields from MPI-ESM for the years 2000 to 4000 and calculated the SMB with the EBM of the MPI-ESM model system. The computed 3-D SMB was then interpolated onto the surface topographies of each model system (see section 2.1.4 for details). Differences between these experiments allow us to isolate the effect of the surface topography on the SMB.

Experiment ID	EBM	Climate forcing	Topography	
EA	AWI-ESM	MPI-ESM	MPI-ESM	EBM effect
EC	CLIMBER-X	MPI-ESM	MPI-ESM	
EM	MPI-ESM	MPI-ESM	MPI-ESM	
CA	AWI-ESM	AWI-ESM	AWI-ESM	Climate forcing effect
CC	AWI-ESM	CLIMBER-X	AWI-ESM	
CM	AWI-ESM	MPI-ESM	AWI-ESM	
TA	MPI-ESM	MPI-ESM	AWI-ESM	Topography effect
TC	MPI-ESM	MPI-ESM	CLIMBER-X	
TM	MPI-ESM	MPI-ESM	MPI-ESM	

Table 2. Overview of the sensitivity experiments aimed at disentangling the effects of different EBMs, ice-sheet topographies and climate models on the simulated SMB of the GrIS. The experiment IDs are constructed by using the first letter of the sensitivity experiments category and the first letter of the respective model system.

3 Results

Forcing the climate-ice sheet models with the future scenarios affects the atmosphere, ocean, land and ice sheets in various ways. Initially, we focus on the overall climate evolution and on regional changes over Greenland. We structure the analysis from the global to the regional scale and commence with the global climate response, followed by the atmospheric fields that determine the SMB of the GrIS. Collectively, these analyses lay the foundation for the key section in which we aim to disentangle the drivers of differences in the ice-sheet response of our three model systems.

3.1 Global and Greenland climate evolution

Global mean near-surface air temperatures respond strongly to the increasing greenhouse gas concentrations in all simulations (Fig. 1a and b). Thereby, MPI-ESM shows the strongest and CLIMBER-X the weakest response. By 2100, global mean near-

https://doi.org/10.5194/egusphere-2026-3384
Preprint. Discussion started: 6 July 2026

surface air temperatures show an increase of 2.4–2.8°C in SSP2-4.5, of 2.8–3.1°C in SSP4-6.0 and 3.6–4.3°C in SSP5-8.5 for the three models and continue to increase thereafter. Although greenhouse gases are reduced after year 2200 in all scenarios, near-surface air temperatures only slowly respond and remain higher than present-day near-surface air temperatures in all models and across all scenarios, consistent with the higher prescribed atmospheric CO_2 concentration. By year 4000, near-surface air temperatures anomalies remain between 2.0–2.8°C in SSP2-4.5, 2.7–3.9°C in SSP4-6.0, and 6.7–11.0°C in SSP5-8.5 higher than PI.

Due to the substantial initial warming, the Atlantic Meridional Overturning Circulation (AMOC) weakens under all SSPs and across all models (Fig. 1c). The amplitude of the initial weakening is similar for all models for the individual scenarios, despite the difference in the resolution of the ocean model components. Only for SSP5-8.5 and CLIMBER-X, the AMOC enters a state where it is persistently collapsed. In all simulations, except SSP5-8.5 in CLIMBER-X and to a lesser extent in MPI-ESM, the AMOC slowly recovers over the course of the simulations and reaches nearly its initial strength. Despite the AMOC slowdown, which reduces the heat transport from the lower to the higher latitudes, regional summer near-surface air temperatures over Greenland increase. At 2100, summer near-surface air temperature anomalies over Greenland are 3.11–3.25°C for SSP2-4.5, 3.33–3.77°C for SSP4-6.0, and 4.23–5.29°C for SSP5-8.5. Summer near-surface air temperatures over Greenland continue to increase thereafter and remain higher than PI values throughout the entire length of the simulations, with temperature anomalies of 2.8–4.8°C for SSP2-4.5, 3.9–8.1°C for SSP4-6.0 and 6.6–28.0°C in SSP5-8.5 at year 4000 (Fig. 1d). An exception presents the SSP5-8.5 CLIMBER-X simulation. Here, summer near-surface temperature anomalies are even slightly lower than the intermediate scenario SSP2-4.5 for AWI-ESM and MPI-ESM. The tapering-off in the summer near-surface temperature warming in the CLIMBER-X SS5-8.5 scenario coincides with the AMOC transitioning into its collapsed state. In addition, the summer near-surface temperature signal in SSP5-8.5 for AWI-ESM and MPI-ESM carries a strong warming signal induced by the substantial lowering in elevation and changes in surface albedo in response to the complete disintegration of the GrIS.

Greenland precipitation increases in all simulations and remains higher throughout all simulations, except for SSP5-8.5 with CLIMBER-X (Fig. 1e). As for the summer near-surface temperature over Greenland, the start of the precipitation decrease in the CLIMBER-X SSP5-8.5 simulation temporally aligns with the collapse of the AMOC. Precipitation changes in AWI-ESM and MPI-ESM are very similar in terms of their magnitude and temporal evolution, although AWI-ESM shows a slightly weaker precipitation increase for SSP2-4.5 than MPI-ESM. For these two models, precipitation increases most strongly under higher emission scenarios. Only CLIMBER-X shows little difference in precipitation over Greenland between scenarios, except for SSP5-8.5 for which precipitation decreases after 2500. The latter can likely be associated with the collapse of the AMOC and changes in regional precipitation patterns. As changes in the precipitation patterns directly affect accumulation over the GrIS these results are further discussed in Section 3.4.

Both, the increase in near-surface air temperatures over Greenland and the increase in precipitation – liquid and solid – ultimately affect the SMB and thereby the volume of the GrIS. Our models project a retreat of the GrIS under all scenarios, which is discussed through the next section.

https://doi.org/10.5194/egusphere-2026-3384
Preprint. Discussion started: 6 July 2026

3.2 Greenland mass loss projections

Despite the different employed model spin-up procedures across the three climate-ice sheet models, which have in common that they aim at producing an equilibrated ice sheet state under PI conditions, all of them produce an ice volume at year 2000 that is within 3% of the ice volume from BedMachine (Morlighem et al., 2017), a high resolution dataset that maps bedrock topography, ice thickness, and surface elevation. All models show a clear single dome structure. However, the maximum elevation of the dome differs. In particular, CLIMBER-X starts off with a single-dome maximum elevation that exceeds the maximum elevation of AWI-ESM and MPI-ESM by a few hundred meters (Figs. 2a,f,k, A2a,f,k, A3a,f,k). Regardless of the emission scenario, all models show a mass loss trend for the GrIS. Sea-level rise contributions by 2100 remain moderate, ranging from 0.03–0.06 m for SSP2-4.5, 0.03–0.08 m for SSP4-6.0, and 0.04–0.11 m SLE for SSP5-8.5. On timescales beyond 2200, ice-mass loss trends accelerate with a sea-level rise contribution of up to 3.50 m by 2500 for SSP5-8.5 (Fig. 1f). This is supported by the corresponding magnitude of ice sheet thinning, exceeding values of 100 m only at year 2300 and beyond. For the highest emission scenario, a complete deglaciation by the year 3,000 is projected by MPI-ESM. Similar deglaciation timescales have also been reported from stand-alone ice sheet simulations for a similar emission scenario (e.g. Aschwanden et al., 2019). Of the three models, except for the SSP2-4.5 scenario, MPI-ESM shows the largest ice mass loss rates, while CLIMBER-X displays the smallest ice mass loss rates across all scenarios. Interestingly, the ice-thinning patterns for each individual model are very distinct (Fig. 2). In AWI-ESM, the ice sheet starts to retreat from all ice-sheet margins but the south-east region of the ice sheet, before the thinning propagates towards the interior of the ice sheet. In comparison, CLIMBER-X shows similar thinning rates much later than AWI-ESM, in agreement with the reduced simulated ice-mass loss. Moreover, the thinning in CLIMBER-X is moving towards the interior from the southern tip of the GrIS. However, in comparison to the other two models, the central dome of the GrIS in CLIMBER-X experiences little thinning, except in SSP5-8.5 after year 2300. In MPI-ESM, the ice-sheet thinning begins at the western side of the ice sheet. From there, thinning propagates across the entire width of the ice sheet in all emission scenarios and results in the separation of the ice sheet into a small ice cap covering the southern tip of Greenland and a larger remnant in the north of Greenland. The different scenarios have a strong effect on the amplitude, but the spatial patterns for the different models remain very similar (compare Fig. 2 with Figs. A2 and A3). To keep the paper concise, we focus here on scenario SSP2-4.5, because mass loss of the GrIS is most similar in all three models.

To investigate the drivers of these differences in the ice-sheet thinning patterns and the importance of individual components of the integrated mass balance of the ice sheet, we use the following equation:

$$\frac{dM}{dt} = \mathrm{SMB} + \mathrm{BMB} - C. \tag{1}$$

Here, $\frac{dM}{dt}$ is the overall ice mass change rate, SMB is the surface mass balance, C represents the calving discharge out of the ice-sheet domain, and BMB is the basal mass balance under ice shelves. We ignore contributions from basal melting under the grounded portions of the ice sheet, as we deem them less important. Since the ice volume trend is small over the PI period, we focus on analysing anomalies to the individual mass balance components (see Eq.1) relative to PI (see Figs. 3 and A4, A5). Across all three models a coherent picture emerges that shows that the overall mass loss is dominated by changes in the SMB. This is in agreement with results from previous studies (e.g. Fyke et al., 2014; Aschwanden et al., 2019; Muntjewerf et al.,

https://doi.org/10.5194/egusphere-2026-3384
Preprint. Discussion started: 6 July 2026

2020; Goelzer et al., 2020; Madsen et al., 2022; Rahlves et al., 2025). The smallest mass loss contribution is provided by basal melting, mainly due to the very limited ice-shelf areas of the GrIS. Ice mass loss due to calving effectively reduces to zero by the year 2300 relative to PI across all models. This reductions is primarily caused by a retreat of marine terminating outlet glaciers onto land (Fig. 2), as the ice sheet retreats inland. The patterns are robust across the different emission scenarios with the only difference being that the magnitudes of the individual mass balance components are enhanced under higher emission scenarios (Figs. A4, A5).

To zoom in further and identify the driving processes behind the SMB changes, we decompose the SMB into its individual components: accumulation and net surface melt, defined here as the sum of surface melt and refreezing. Similar to the overall mass budget, a clear picture emerges that SMB changes are primarily driven by changes in net surface melt. In all three models and across all emission scenario, the changes in net surface melt closely track the changes in SMB, underlining the overwhelming importance of net surface melt evolution for the future of the GrIS. While net surface melt increases almost immediately in all models and across all emission scenarios, the response of accumulation is more varied – both across models but also emission scenarios (Fig. 3). The general trend, particularly for AWI-ESM and CLIMBER-X, but also in parts for MPI-ESM, is an initial increase in accumulation. The duration of the increase varies from scenario to scenario, but tends to persist for a longer period in the lower emission scenarios. For example, CLIMBER-X shows a positive accumulation anomaly throughout the SSP2-4.5 simulation, albeit of small magnitude, while at the other end of the spectrum the increase in accumulation of MPI-ESM does not even last 100 years. The likely reason for this is that summer near-surface air temperatures are close to the freezing point in MPI-ESM and even small increments of warming reduce the fraction of the precipitation that falls as snow. The response of AWI-ESM lies somewhere in between the two end member models.

3.3 Comparison of SMBs with GrSMBMIP

Considering the importance of the SMB as critical driver for the future evolution of the GrIS, we compare SMBs computed by our three models with models that participated in the Greenland Ice Sheet Surface Mass Balance Intercomparison Project (GrSMBMIP) for the time period 1980–2012 (Fettweis et al., 2020). GrSMBMIP compared SMB fields across 13 models of different complexity, spatial resolution, and spatial coverage. Therefore, it provides a good benchmark for our coupled models. Naturally, to keep computational demands manageable for millennial-timescale simulations, the native resolution of the forcing for the EBMs in the coupled climate-ice sheet models is much coarser than for regional climate models. Unlike regional climate models, however, our global climate models provide a physically consistent framework and do not rely on external forcing at the domain boundaries. Despite these significant differences, all three climate-ice sheet models are within the spread of the mean SMB distribution with elevation (henceforth: hypsometric SMB) of the GrSMBMIP models (Fig 4a). While AWI-ESM tends more towards the models of GrSMBMIP with strong melting, CLIMBER-X and MPI-ESM lie on the other end of the spectrum. This is also illustrated by the elevation threshold at which the mean SMB per elevation bin turns negative. Here, AWI-ESM crosses this threshold at ∼1440 m, MPI-ESM at ∼850 m, and CLIMBER-X at ∼540 m. Moreover, it is noticeable, both for our models but also for models of the GrSMBMIP, that there is little variation of the SMB at higher surface elevations (>1,500 m, Fig 4a), where the SMB is dominated by accumulation and net surface melt is rare. The spread significantly widens

https://doi.org/10.5194/egusphere-2026-3384
Preprint. Discussion started: 6 July 2026

in the ablation zone of the GrIS. This explains in large part the different future trajectories, as net surface melt is the dominant driver for the future evolution of the GrIS. Of course, the mean hypsometric SMB only provides an incomplete picture, as the surface topography of the ice sheet as well as the extent of the ice sheet play important roles. Unlike in GrSMBMIP, we do not interpolate the SMB onto a common surface topography and ice sheet mask. Hence, differences between our three models and the GrSMBMIP models increase for the integrated hypsometric SMB per elevation bin (Fig. 4g), while the spread across the GrSMBMIP models remains in a similar range. In comparison to the mean hypsometric SMB, differences in the integrated hypsometric SMB are not limited to the ablation zone of the GrIS, but, in particular for MPI-ESM and AWI-ESM, also spread into higher surface elevations between 2000–2750 m. This corresponds to regions where surface topography between MPI-ESM, AWI-ESM, and the GrSMBMIP models differs the most, demonstrating the effect of different ice sheet surface topographies on the derived SMBs.

3.4 Potential drivers of different surface mass balance trajectories

The SMB in coupled climate-ice sheet models is mainly determined by the climate forcing, the EBM, and the surface topography of the ice sheet. First, we turn our attention to some of the key variables of the climate forcing, precipitation – liquid and solid – and near-surface air temperatures. Particularly relevant for the GrIS are summer (JJA) near-surface air temperatures, as these determine the length and intensity of the melt season. Starting from the large-scale perspective, global mean near-surface air temperatures across the three models are very similar for the lower SSP2-4.5 and SSP4-6.0 emission scenarios. Only for the high SSP5-8.5 emission scenarios do differences across the models exceed the 1 °C threshold (Fig 1b). Similar trends are visible in the mean summer near-surface air temperatures over Greenland, where differences become large (>20 °C) in the SSP5-8.5 emission scenario. However, it is worth noting that most of these differences are due to the differing ice-sheet extents and elevation across our models. Still, even though differences are smaller for SSP2-4.5 and SSP4-6.0, it is evident that both AWI-ESM and MPI-ESM, the two models projecting larger GrIS mass loss, display higher mean summer near-surface air temperatures. At least for MPI-ESM, this pattern is corroborated by the 2D spatial pattern (Fig. 5). Here, MPI-ESM shows the warmest summer near-surface air temperatures over the ice sheet, in agreement with the result that MPI-ESM also predicts the largest ice-mass loss in the future. For the other two models, the analysis becomes more complicated. For example, despite AWI-ESM projecting ice-mass loss of similar magnitude to MPI-ESM, AWI-ESM shows the coldest near-surface air temperatures from all models over the interior of the ice sheet. However, it also exhibits the highest near-surface air temperatures of all models in the immediate vicinity of the ice sheet (Figs. 5, A8, A9). Qualitatively, this matches the near-symmetrical simulated marginal ice-sheet retreat pattern in AWI-ESM (Fig. 2b-e). From the near-surface air temperature alone, it remains unclear why CLIMBER-X simulates the smallest ice mass loss rates for the GrIS. A clear distinction of CLIMBER-X is that the ice-sheet topography is several hundred meters higher than in AWI-ESM and MPI-ESM, especially in the interior of the ice sheet. The overall proportion of the area located below an elevation of 2,000 m is distinctly lower for CLIMBER-X, than for MPI-ESM. AWI-ESM again is between these two end-member models. This results in less accumulation in the upper reaches of the ice sheet over the course of the simulation, but more importantly limits the area exposed to net surface melt and consequently the total amount of net surface melt. Ultimately, it becomes evident that the combination of climate forcing, EBM, and surface

https://doi.org/10.5194/egusphere-2026-3384
Preprint. Discussion started: 6 July 2026

topography determine the overall SMB evolution. Nonetheless, because they all interact with each other, it is difficult to gauge the individual importance of these three key factors based on the scenario projections. This is why we performed additional sensitivity experiments that are specifically tailored towards isolating the importance of each of these three key factors.

3.5 Isolating the importance of EBM, climate forcing, and surface topography for SMB evolution

With the aid of the additional sensitivity experiments described in section 2.2.2, we aim to determine the leading drivers for the simulated changes in SMB. In total, we investigate three different effects: (i) different EBMs, (ii) different climate forcings, and (iii) different surface topographies. The abbreviations of the sensitivity experiments are composed of the first letter of the category of the sensitivity experiment (EBM, climate forcings, topography) and the first letter of the respective model system. For example, for the EBM sensitivity experiment with the AWI-ESM model the experiment ID is EA (see Table 2 and Figs. 7–9). The sensitivity experiments are performed by varying only one of the three input parameters (e.g. surface topography) while keeping the other two parameters fixed (e.g. EBM and climate forcing). We restrict our analysis to the SSP2-4.5 scenario, but the other scenarios are provided as Appendix Figures A6 and A7. Mostly, because the higher emission scenarios do not add any insights as they show similar results with enhanced magnitude compared to SSP2-4.5. Of the three tested drivers, it becomes evident that different surface topographies cause the smallest differences in SMB. This holds true for both the spread of the mean SMB per elevation bin, but also for the spread of integrated SMB per elevation bin (Fig. 6c, i). The elevation threshold, at which the mean SMB per elevation bin crosses the zero-line, is within ∼85 m. In addition, the spatial pattern of the SMB and its individual components, net surface melt and accumulation, also show almost identical spatial structures for the different surface topography simulations across the GrIS (Figs. 7, 8, 9). Using different EBMs or climate forcings results in considerably larger differences in simulated SMB across models. The analysis of the hypsometric profile reveals that different climate forcings show the strongest response, both in the mean and integrated SMB measures, but also in the spread in elevation at which the mean SMB crosses the zero-line (Fig. 6). It covers an elevation range of ∼680 m for the different climate forcings and ∼500 m for the different EBMs. The spatial patterns show much more variability across the SMB, net surface melt and even accumulation. Particularly, the CLIMBER-X climate forcing displays structural differences in SMB and accumulation fields, consistent with the differences in near-surface air temperature and precipitation patterns (see section 3.1). For the climate forcing simulation with MPI-ESM and AWI-ESM, this is restricted to the accumulation field. Similar structural differences can be found in the simulated SMB fields from the sensitivity simulations with different EBMs. Even with the additional sensitivity simulations, it remains challenging to distinctly conclude whether the EBM or the climate forcing are more critical for the SMB evolution. However, to provide a more concrete example about the potential magnitude of the changes, we can compare the sensitivity experiment with the EBM, climate forcing, and surface topography of MPI-ESM (Fig. 7g, EM) with the experiment that utilizes the CLIMBER-X EBM and climate forcing and surface topography from MPI-ESM (Fig. 7d, EC). The only difference between the two sensitivity simulations is the choice of the EBM. By only switching the EBM, we transition from a SMB field experiencing considerable net surface melt in the marginal regions of the ice sheet to a SMB field that shows almost no negative SMB regions across the ice sheet (Fig. 7d, g). In other words, by switching the EBM, we change the SMB field from exhibiting the least positive integrated SMBs across all sensitivity simulations to

https://doi.org/10.5194/egusphere-2026-3384
Preprint. Discussion started: 6 July 2026

the SMB field with the most positive integrated SMB of the sensitivity simulations. This illustrates the magnitude of changes that different EBMs can cause for the SMB of the GrIS. By extending the analysis and comparing AWI-ESM (Fig. 7a) and MPI-ESM (Fig. 7g) it becomes evident that the EBM of MPI-ESM shows larger net surface melting rates, particularly between 500 and 2000 m (Fig. 6a). On the other side, the climate forcing from AWI-ESM (Fig. 7b) produces considerably stronger net surface melting than the forcing from MPI-ESM (Fig. 7h). Thus, the differences in SMB due to climate forcing and EBM tend to compensate each other.

4 Discussion

Ice sheets are a slow responding climate component, particularly in comparison to the atmosphere and the ocean. As a result, ice-sheet projections transition much more slowly mathematically from an initial value problem, dominated by the initial state of the ice sheet, to a boundary value problem, dominated by climate forcing. This is relevant because it emphasises the initial state of the ice sheet as a key uncertainty in future ice sheet projection (e.g. Arthern and Gudmundsson, 2010; Aðalgeirsdóttir et al., 2014; Aschwanden et al., 2021). As long spin-up simulations typically lead to differences between simulated and observed ice-sheet geometries, data assimilation techniques are often preferred over spin-up techniques, especially for projections spanning only a few centuries (Goelzer et al., 2018). However, the results of our sensitivity simulations show that at least the initial geometry, a key component of the initial ice-sheet state, plays a minor role relative to the choice of the EBM and the climate forcing in coupled climate-ice sheet projections of the GrIS. Considering that data assimilation techniques typically only capture memory effects that cover the extent of the observational period and show strong initial model drifts, the finding that the initial geometry of the ice sheet seems to be less critical is encouraging, particularly for models covering millennial timescales. Moreover, it indicates that initial state uncertainty due to varying ice-sheet geometries is likely not the dominating source of uncertainty in sea-level rise projections from coupled climate-ice sheet models. A distinct advantage of our model simulations, particularly in light of the millennial timescales examined here, is that they do not make use of so called "anomaly forcing" that is routinely employed in stand-alone ice sheet simulation (Aschwanden et al., 2019; Goelzer et al., 2020; Seroussi et al., 2020; Goelzer et al., 2025; Rahlves et al., 2025), but has also been used in coupled climate-ice sheet simulations (Ridley et al., 2005; Mikolajewicz et al., 2007b; Vizcaíno et al., 2008; Ganopolski et al., 2010). The "anomaly" forcing effectively bias-corrects relevant climate forcing fields against some baseline. This implicitly assumes that the underlying spatial pattern of the bias correction does not change over the course of the simulation period. While this may be a justifiable assumption for decadal to century timescales, it is likely invalid for simulations spanning several millennia involving major changes of the ice sheet geometry.

Broadly speaking, our sea-level rise projections until 2100 are in a similar range as reported from ISMIP6 (Goelzer et al., 2018, 2025), and also from other ensemble simulations with stand-alone ice-sheet models (Aschwanden et al., 2019; Rahlves et al., 2025). On this relatively short timescale, the maximum sea-level rise projection is 0.11 m for year 2100 and SSP5-8.5. However, large-scale ice-sheet changes start to occur on timescales beyond 2100, in agreement with previous studies (Vizcaino et al., 2015; Haubner et al., 2026). This suggests that the inherent timescale of large-scale ice-sheet changes for the GrIS is

https://doi.org/10.5194/egusphere-2026-3384
Preprint. Discussion started: 6 July 2026

more than a century. We therefore argue that ice-sheet climate interactions are likely to be less important for the global climate evolution over the next century than on millennial timescales (Vizcaino et al., 2015; Haubner et al., 2026).

The projected mass loss of the GrIS in our simulations is controlled by the SMB (Fig. 3). More specifically, changes in net surface melt determine the magnitude of ice-mass loss. The magnitude of net surface melt is closely linked to near-surface air temperature over the GrIS. This is supported by the fact that for our model intercomparison, the model with the highest warming over Greenland also projects the largest ice-sheet mass loss (Fig. 1). Here, it is important to note that especially for the lower emission scenarios SSP2-4.5 and SSP4-6.0, average global near-surface air temperature differences between the models are small compared to the critical summer near-surface air temperature differences over Greenland. This indicates that average global near-surface air temperature is not the best indicator for the expected ice-sheet response. In a similar vein, the Equilibrium Climate Sensitivity (ECS) has been previously used to explain greater GrIS mass loss in the Coupled Model Intercomparison Project 6 (CMIP6) models compared to CMIP5 (Hofer et al., 2020). However, our simulations highlight that, while ECS is certainly an important factor, it is by no means as overwhelmingly important as previously indicated. For example, CLIMBER-X and AWI-ESM almost have identical ECS, but show very different GrIS ice-sheet responses. Unlike in most stand-alone ice-sheet models or climate models without interactive ice sheets, the near-surface air temperature signal is modulated by the EBM implementation and tuning. As illustrated (Fig. 1), the EBM can offset several degrees of near-surface air temperature differences in specific cases and therefore still produce similar SMBs in coupled climate-ice sheet models for the GrIS. The dominance of near-surface air temperature is further illustrated by the observation that the net surface melt closely tracks the overall SMB evolution in all emission scenarios (Fig. 3). Particularly, in the high emission scenario SSP5-8.5, the near-surface air temperature signal of more than 6°C in the global average, dominates the global climate response as well as the ice-sheet response, underlining the critical role of the characteristics of the climate model for the future evolution of the GrIS. The strong near-surface air temperature signal in the SSP5-8.5 scenario largely overprints any potential climate-ice sheet feedbacks. Even the simulated drastic AMOC slowdown in CLIMBER-X does not leave a global signal in the near-surface air temperature evolution. However, it largely explains the regionally much different near-surface air temperature response over the GrIS in comparison to MPI-ESM and AWI-ESM, where reduction in AMOC strength is much weaker and where AMOC eventually slowly recovers to its initial strength. Considering the overwhelming importance of the climate in SSP5-8.5, we hypothesise that high-emission scenarios may not be ideally suited to investigate climate-ice sheet interactions for the GrIS. This may also explain why a previous study using a coupled climate-ice sheet model found little difference in simulated climate patterns with and without dynamic ice sheets (Haubner et al., 2026).

5 Conclusions

We have presented millennial-timescale projections of the GrIS with three different coupled climate-ice sheet models. While the contribution to sea-level rise projections across the models is small by 2100, ranging from 0.03-0.11 m, it is the timescales beyond 2100, when sea-level rise projections start to diverge. At year 3,000, differences reach values as high as ∼4.4 m in SSP5-8.5 across our models. This emphasises the value of simulations covering periods beyond 2100 and 2300, especially

https://doi.org/10.5194/egusphere-2026-3384
Preprint. Discussion started: 6 July 2026

for the investigation of long-term climate-ice sheet feedbacks. All three coupled climate–ice sheet models identify the SMB, particularly net surface melt, as the primary driver of future ice-sheet mass loss. However, the magnitude of the SMB-driven mass loss differs substantially among the models. Our dedicated sensitivity simulations reveal that climate forcing and choice of EBM are more critical than ice-sheet topography after model spin-up in explaining the simulated diverging GrIS trajectories, particularly on millennial timescales. Therefore, our results underline that reliable long-term projections of the GrIS critically depend on improving the representation of the surface energy balance and climate forcing, rather than on refining initial ice-sheet topography alone.

https://doi.org/10.5194/egusphere-2026-3384
Preprint. Discussion started: 6 July 2026

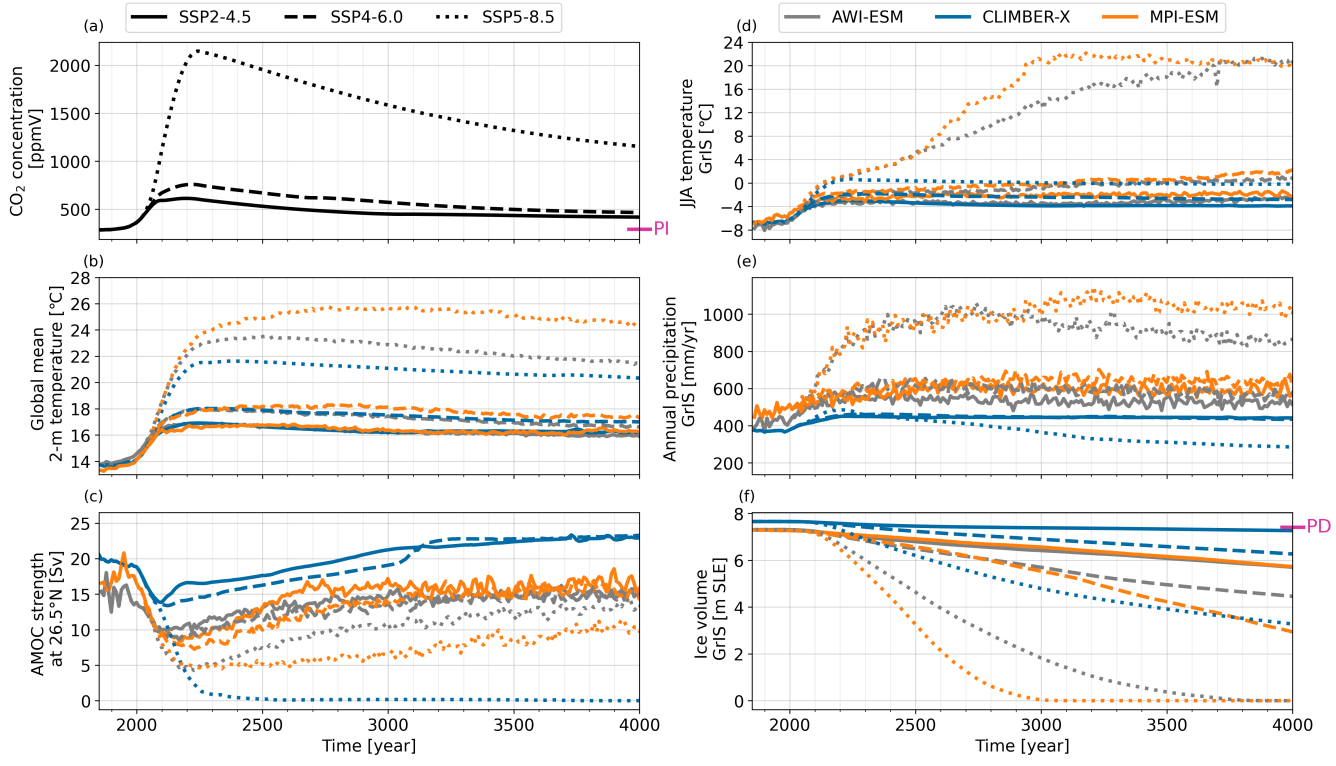

Figure 1. Timeseries of a) atmospheric CO_2 concentration, b) global mean near-surface air temperature, c) maximum AMOC strength at 26.5°N as well as mean d) summer near-surface air temperature and e) total precipitation over the Greenland ice sheet and f) Greenland ice volume for all models and all scenarios. The pink line in a) marks the PI CO_2 concentration and in f) the present-day Greenland ice volume as observed through BedMachine v3 (Morlighem et al., 2017). Anomalies relative to PI are shown in Appendix Fig. A1.

https://doi.org/10.5194/egusphere-2026-3384
Preprint. Discussion started: 6 July 2026

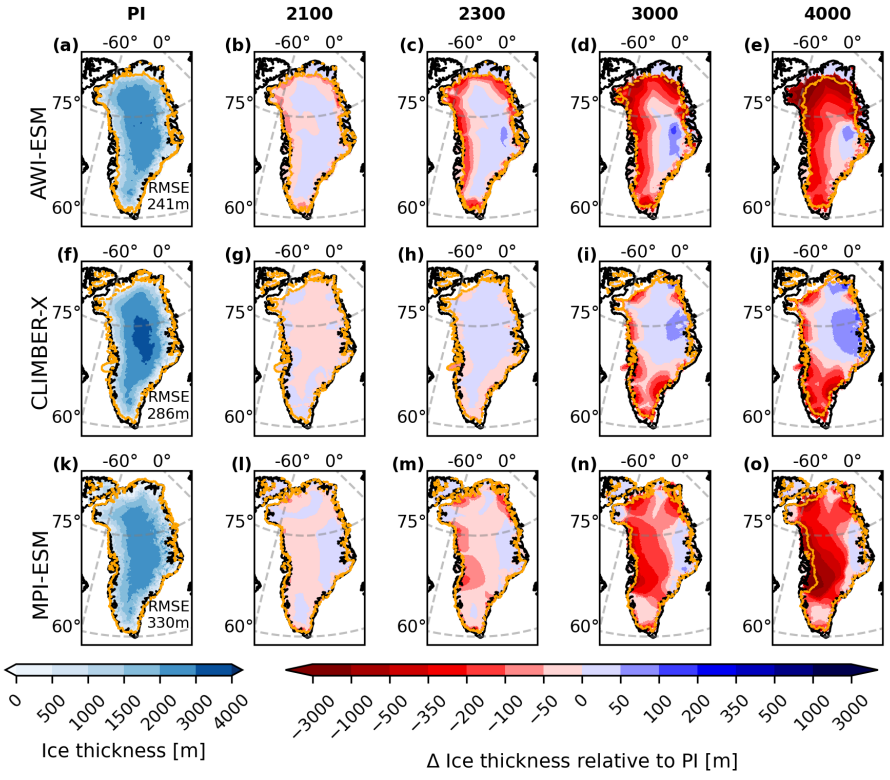

Figure 2. Maps of ice thickness distribution for the Greenland ice sheet from (a) AWI-ESM, (f) CLIMBER-X, (k) MPI-ESM for the pre-industrial (PI) period (1850–1949). RMSEs are calculated with respect to the Bedmachine v3 dataset (Morlighem et al., 2017). Ice thickness changes relative to PI at specific time slices for (b-e) AWI-ESM, (g-j) CLIMBER-X, and (l-o) MPI-ESM for the emission scenario SSP2-4.5. The orange line approximates the ice extent at the specific time slices. Note the non-linear colourscales. Model output is from decadal mean data.

https://doi.org/10.5194/egusphere-2026-3384
Preprint. Discussion started: 6 July 2026

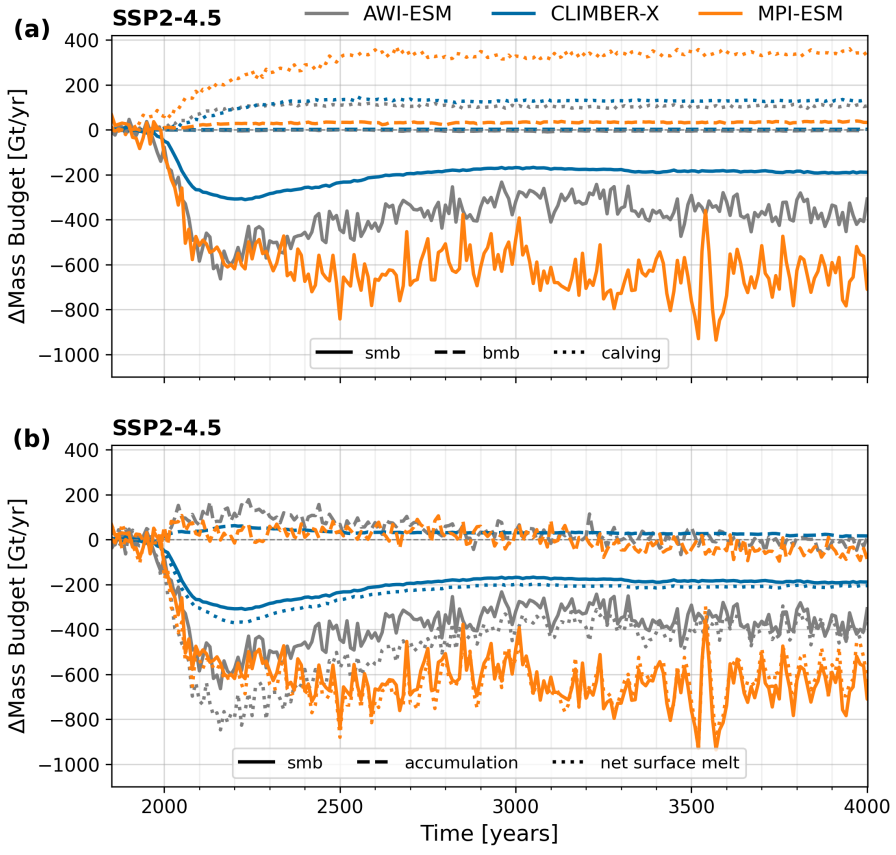

Figure 3. Timeseries of changes for all models relative to PI for (a) ice mass budget components, as defined in Eq. 1, and (b) individual surface mass balance components of the Greenland ice sheet for the emission scenario SSP2-4.5. The abbreviations are as follows: smb=surface mass balance and bmb=basal mass balance under ice shelves. Note that the smb lines in (a) and (b) are equivalent for each of the three models. Model output is from decadal mean data.

https://doi.org/10.5194/egusphere-2026-3384
Preprint. Discussion started: 6 July 2026

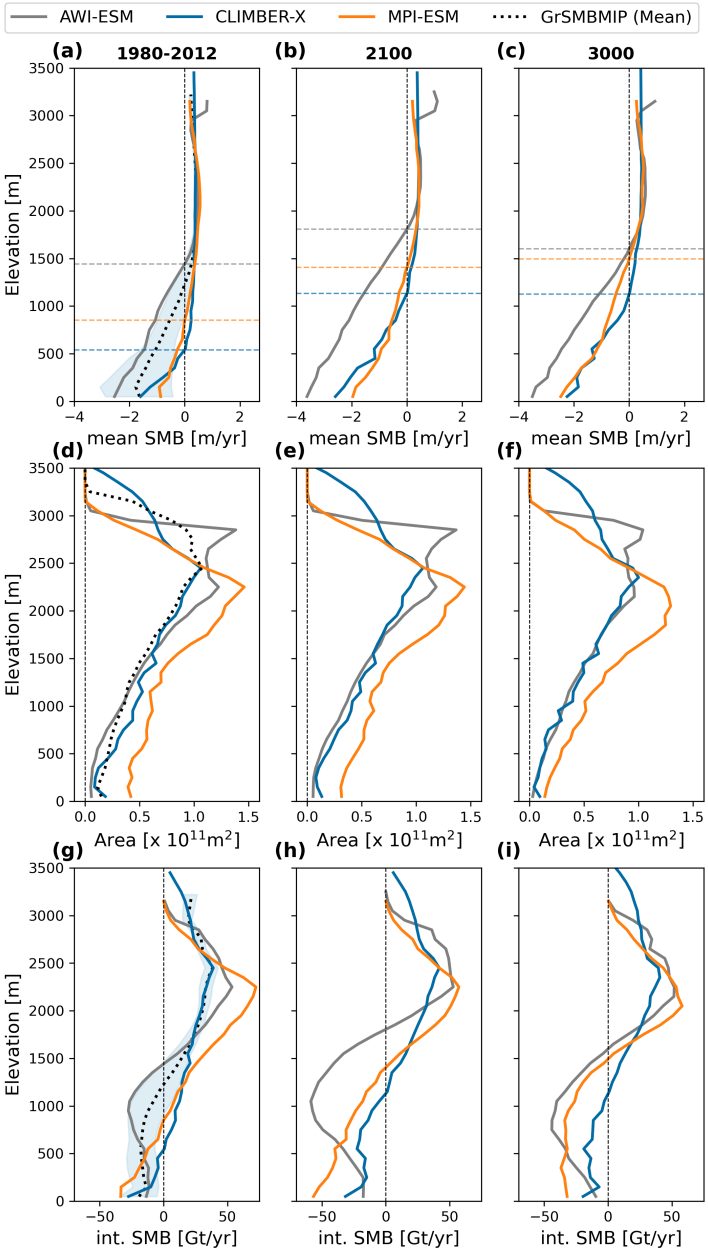

Figure 4. Hypsometric profiles for the SSP2-4.5 scenario of the (a-c) mean surface mass balance (SMB), (d-f) surface area, and (g-i) integrated SMB for the time slices 1980–2012, 2100, 3000, respectively. The integrated SMB (g-i) is the product of mean SMB (a-c) and surface area (d-f). Blue shading in (a) and (g) show the spread of all models that participated in the GrSMBMIP intercomparison (Fettweis et al., 2020). Note that there is no spread in (d), because all models of the GrSMBMIP used the same surface topography. Horizontal coloured dashed lines approximate the elevation when the mean surface mass balance becomes negative for each model. The profiles are plotted using 100 m elevation bins. Model output is from decadal mean data.

https://doi.org/10.5194/egusphere-2026-3384
Preprint. Discussion started: 6 July 2026

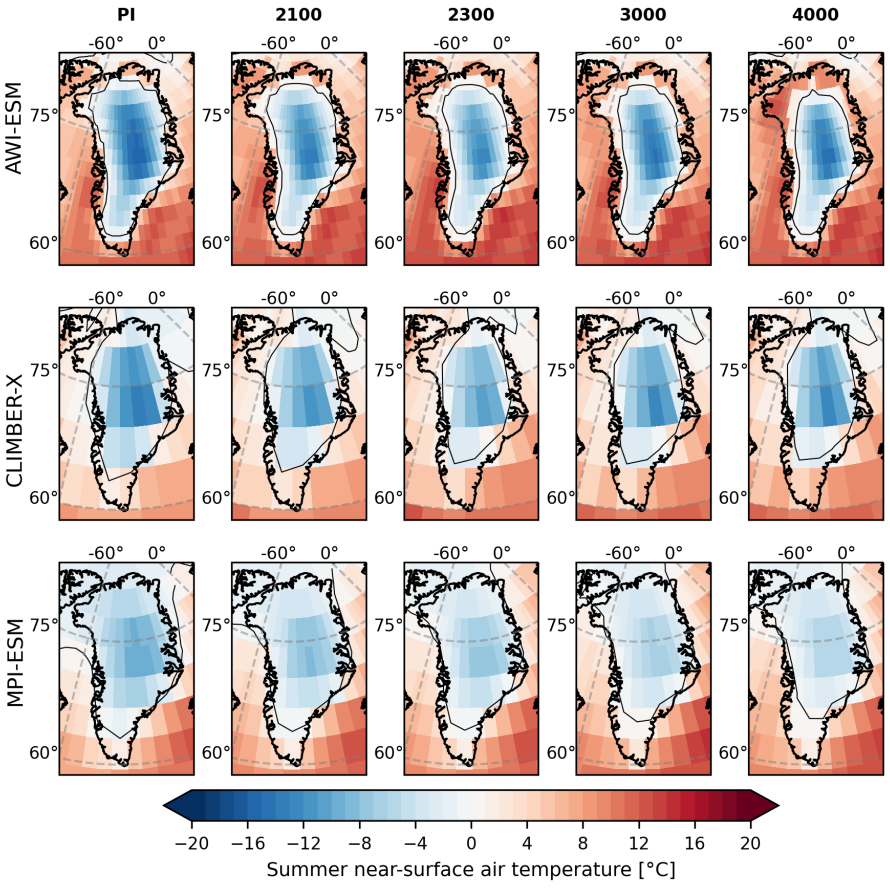

Figure 5. Maps of summer (JJA) near-surface air temperature over Greenland at selected time slices for the SSP2-4.5 emission scenario for all three models. The black contour line marks where the near-surface air temperature is 0°C.

https://doi.org/10.5194/egusphere-2026-3384
Preprint. Discussion started: 6 July 2026

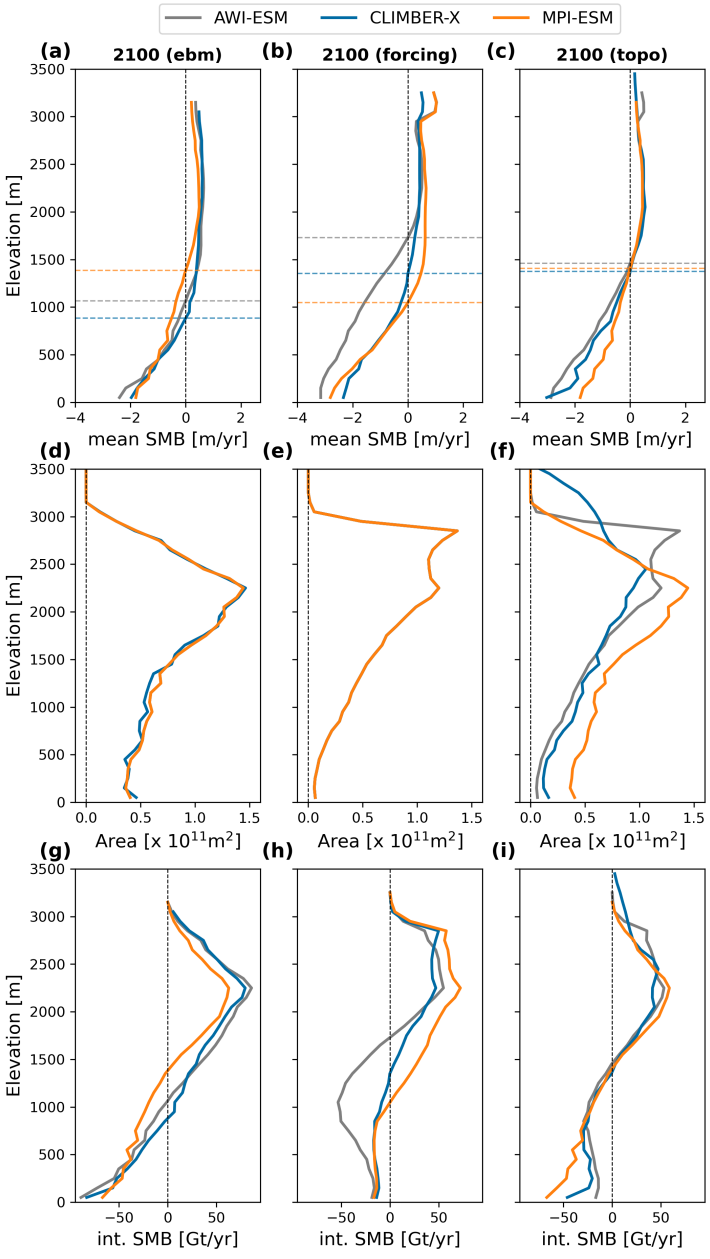

Figure 6. Hypsometric profiles at year 2100 for (a-c) mean surface mass balance (SMB), (d-f) surface area, and (g-i) integrated surface mass balance for different EBMs (left column), different climate forcings (middle column), and different surface topographies (right column). Horizontal coloured dashed lines approximate the elevation when the mean surface mass balance becomes negative for each model. The profiles are plotted using 100 m elevation bins. Note that in panels (d) and (e) all models use the same surface topography. The small deviations in (d) are due to the different horizontal ice-sheet resolution used in CLIMBER-X. Model output is from decadal mean data.

https://doi.org/10.5194/egusphere-2026-3384
Preprint. Discussion started: 6 July 2026

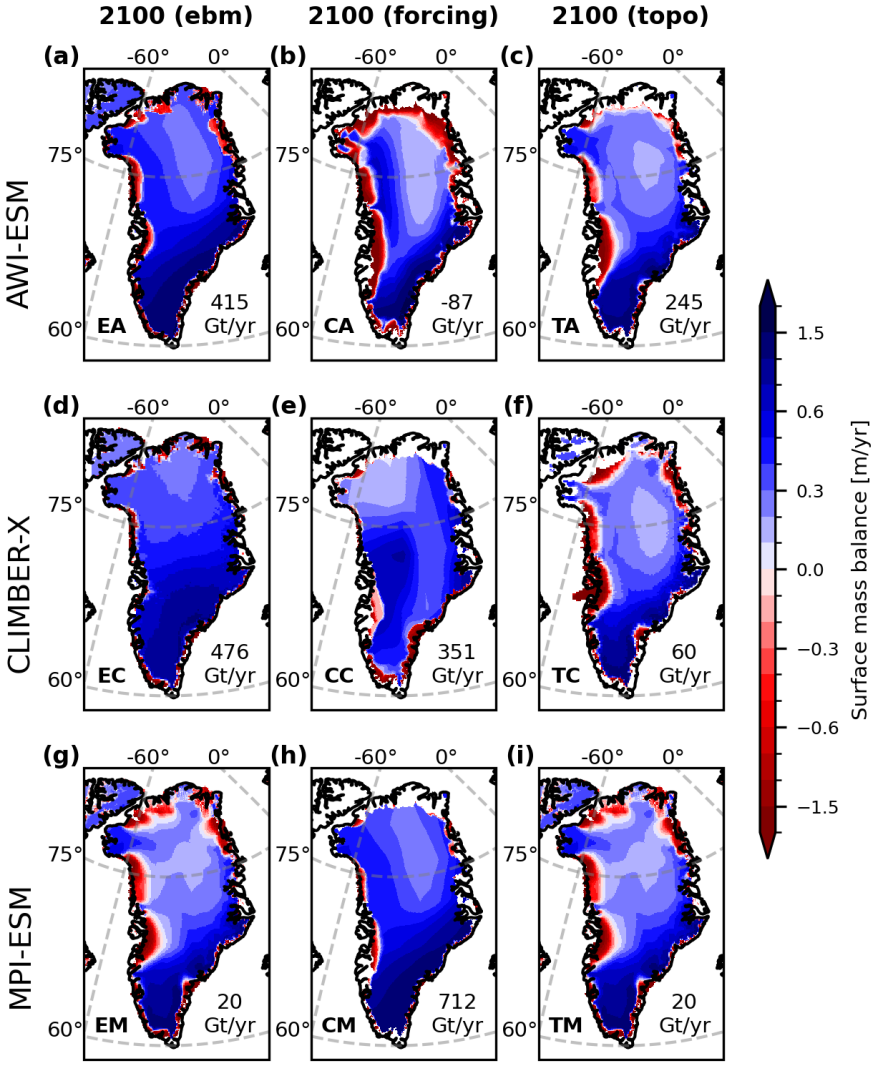

Figure 7. Maps of surface mass balance distribution for the Greenland ice sheet at year 2100 for the SSP2-4.5 emission scenario and for (a, d, g) different EBMs, (b, e, h) different climate forcing, and (c, f, i) different surface topographies. The experiment ID is shown in the lower left corner (see Table 2). The integrated surface mass balance is shown in the lower right of each subplot. Model output is from decadal mean data.

https://doi.org/10.5194/egusphere-2026-3384
Preprint. Discussion started: 6 July 2026

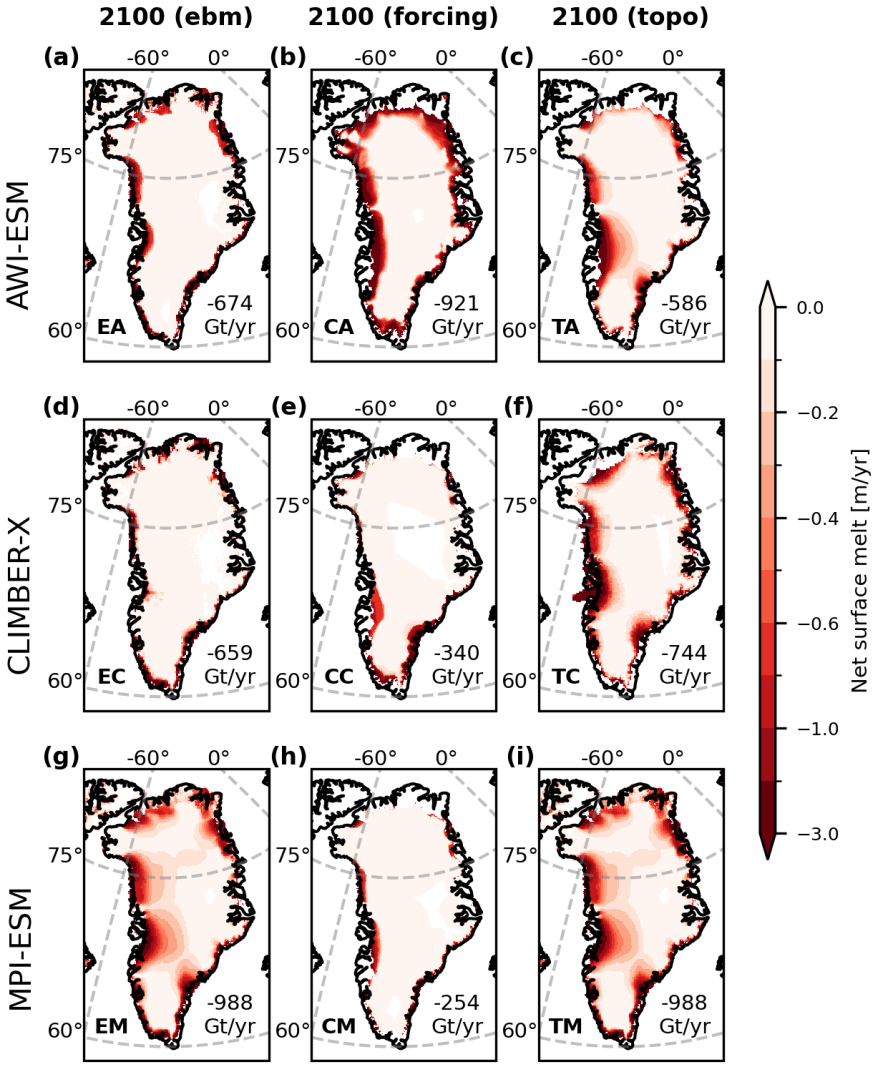

Figure 8. Similar to Fig. 7, but for net surface melt.

https://doi.org/10.5194/egusphere-2026-3384
Preprint. Discussion started: 6 July 2026

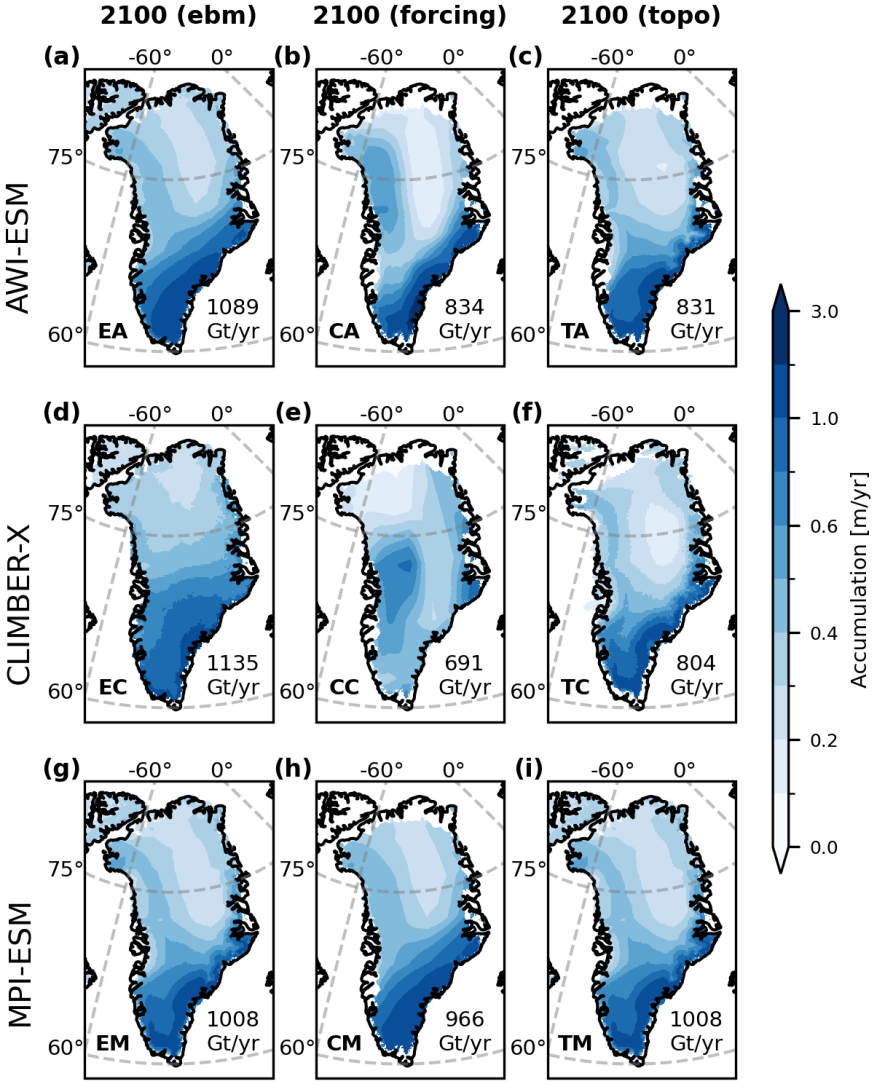

Figure 9. Similar to Fig. 7, but for accumulation.

https://doi.org/10.5194/egusphere-2026-3384
Preprint. Discussion started: 6 July 2026

Appendix A: Figures

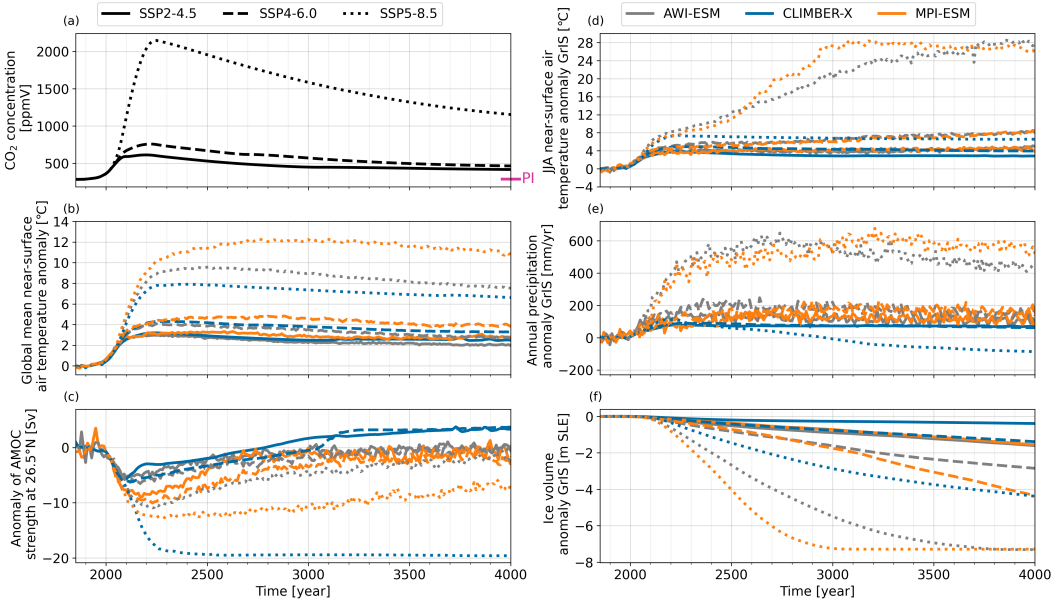

Figure A1. Similar to Fig. 1, but shown are anomalies relative to PI except for the CO_2 concentrations.

https://doi.org/10.5194/egusphere-2026-3384
Preprint. Discussion started: 6 July 2026

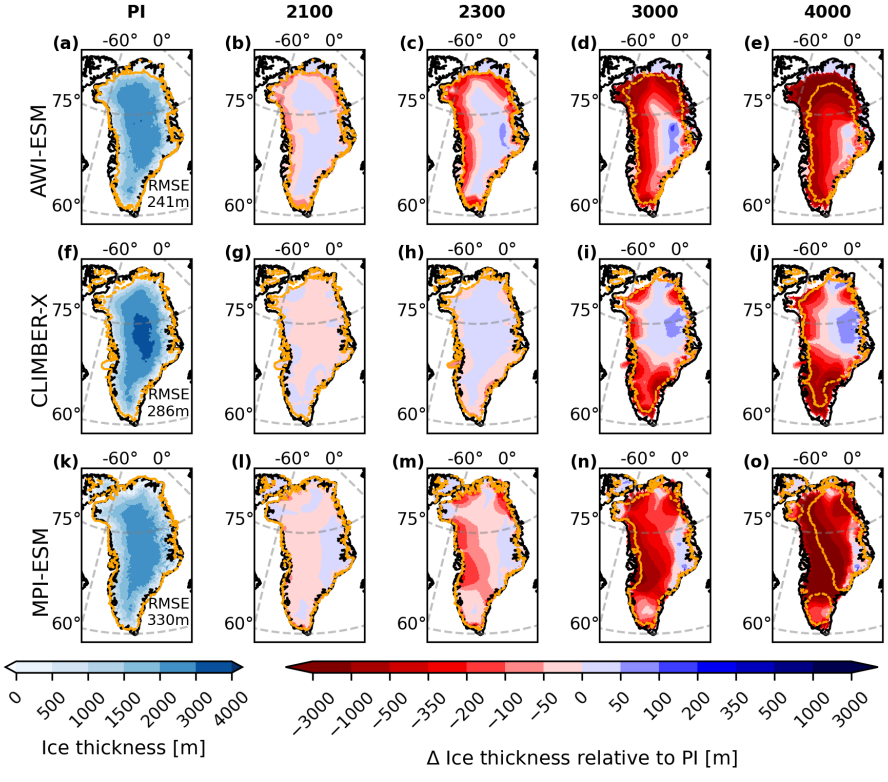

Figure A2. Similar to Fig. 2, but for SSP4-6.0.

https://doi.org/10.5194/egusphere-2026-3384
Preprint. Discussion started: 6 July 2026

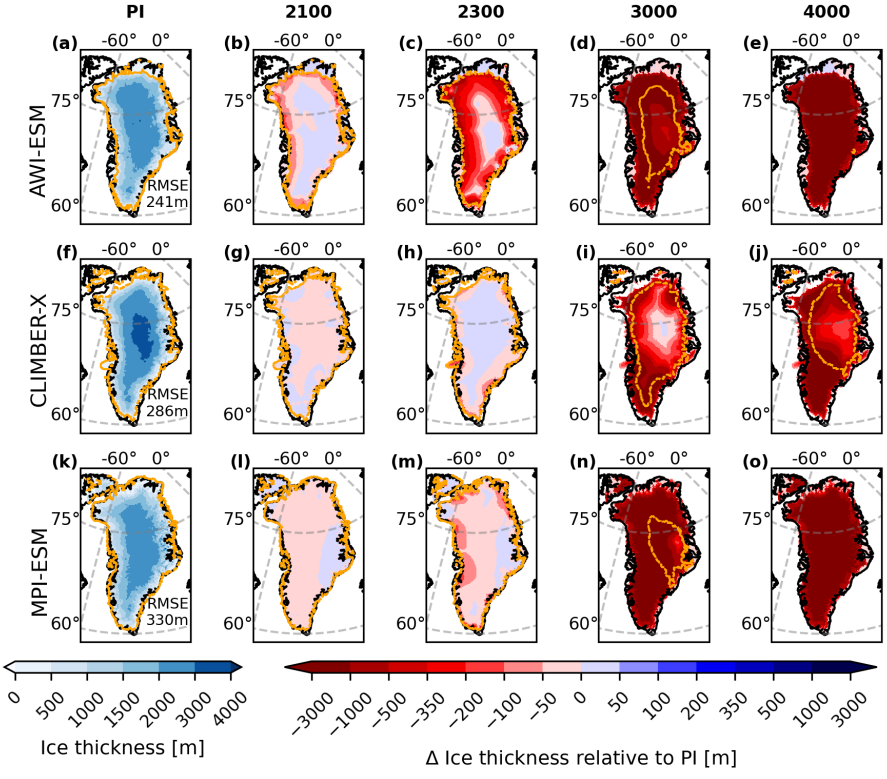

Figure A3. Similar to Fig. 2, but for SSP5-8.5.

https://doi.org/10.5194/egusphere-2026-3384
Preprint. Discussion started: 6 July 2026

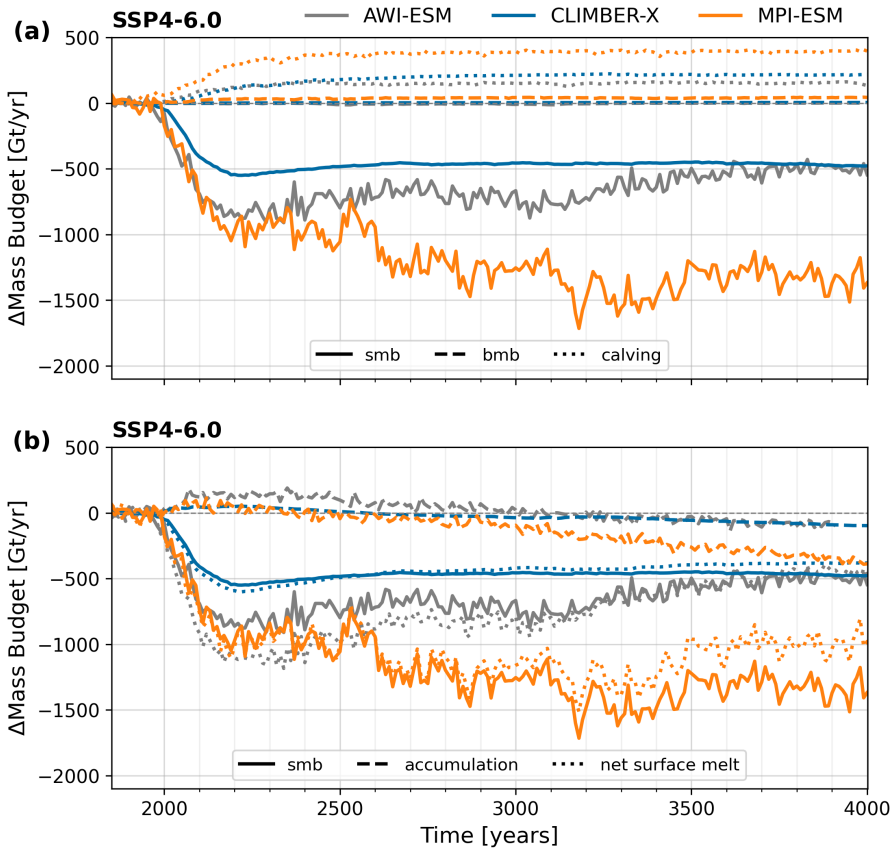

Figure A4. Similar to Fig. 3, but for SSP4-6.0.

https://doi.org/10.5194/egusphere-2026-3384
Preprint. Discussion started: 6 July 2026

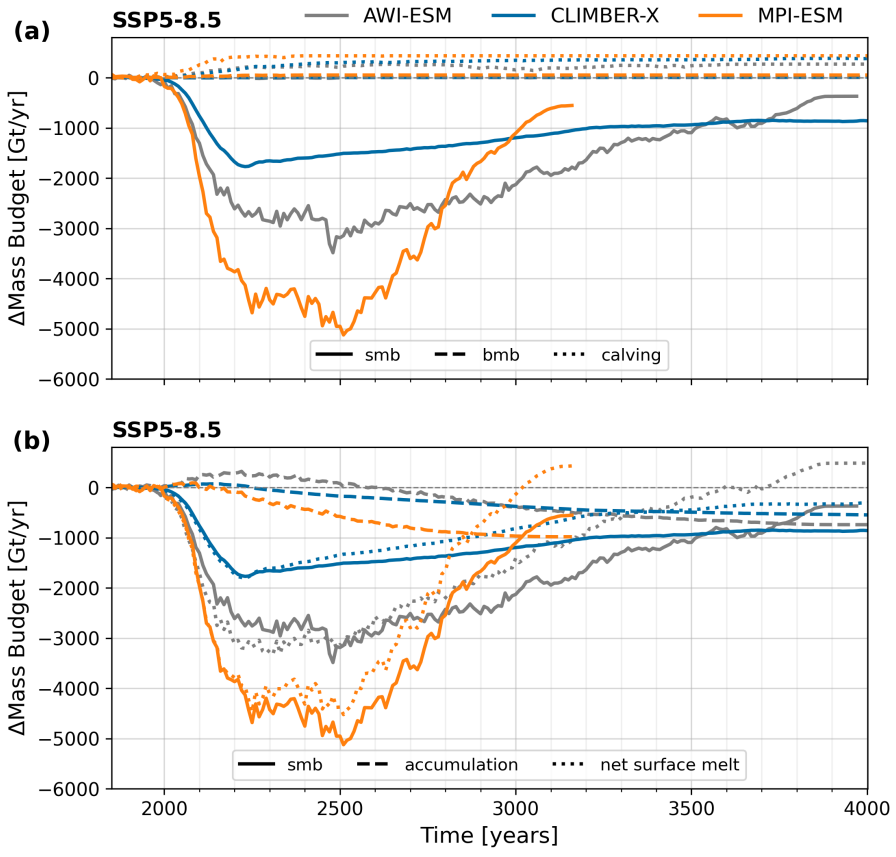

Figure A5. Similar to Fig. 3, but for SSP5-8.5. The lines for MPI-ESM do not cover the entire simulation because the Greenland ice sheet completely disintegrates before.

https://doi.org/10.5194/egusphere-2026-3384
Preprint. Discussion started: 6 July 2026

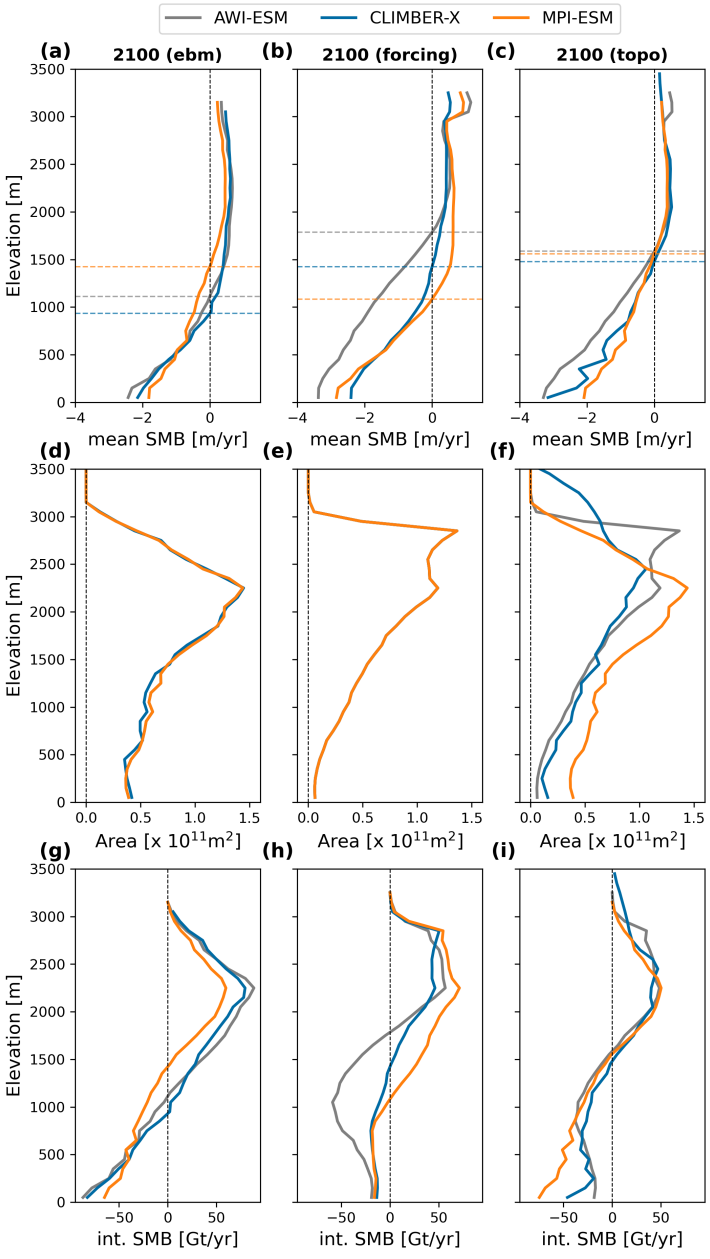

Figure A6. Similar to Fig. 6, but for SSP4-6.0.

https://doi.org/10.5194/egusphere-2026-3384
Preprint. Discussion started: 6 July 2026

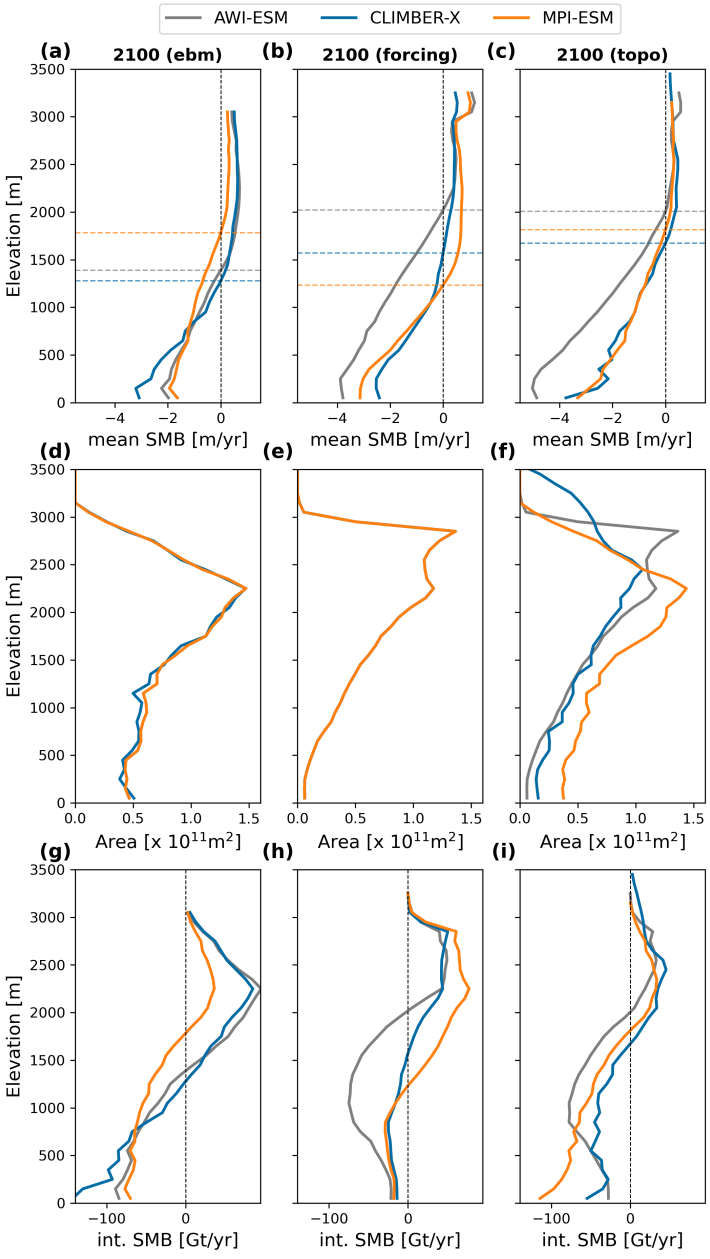

Figure A7. Similar to Fig. 6, but for SSP5-8.5.

https://doi.org/10.5194/egusphere-2026-3384
Preprint. Discussion started: 6 July 2026

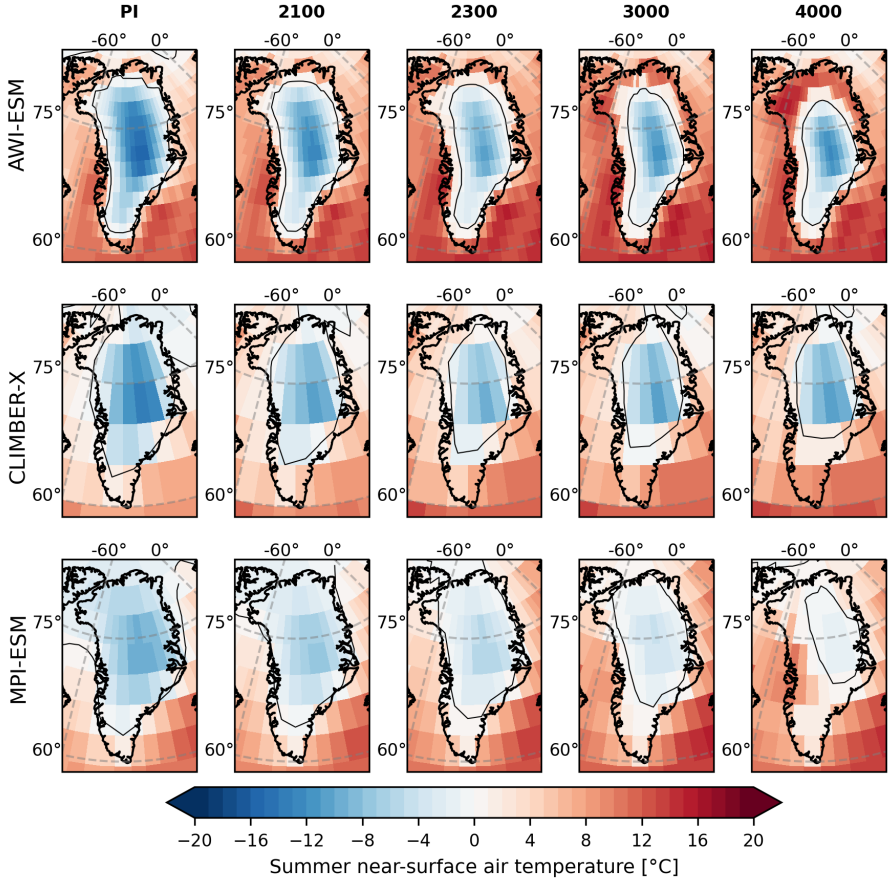

Figure A8. Similar to Fig. 5 but for SSP4-6.0.

https://doi.org/10.5194/egusphere-2026-3384
Preprint. Discussion started: 6 July 2026

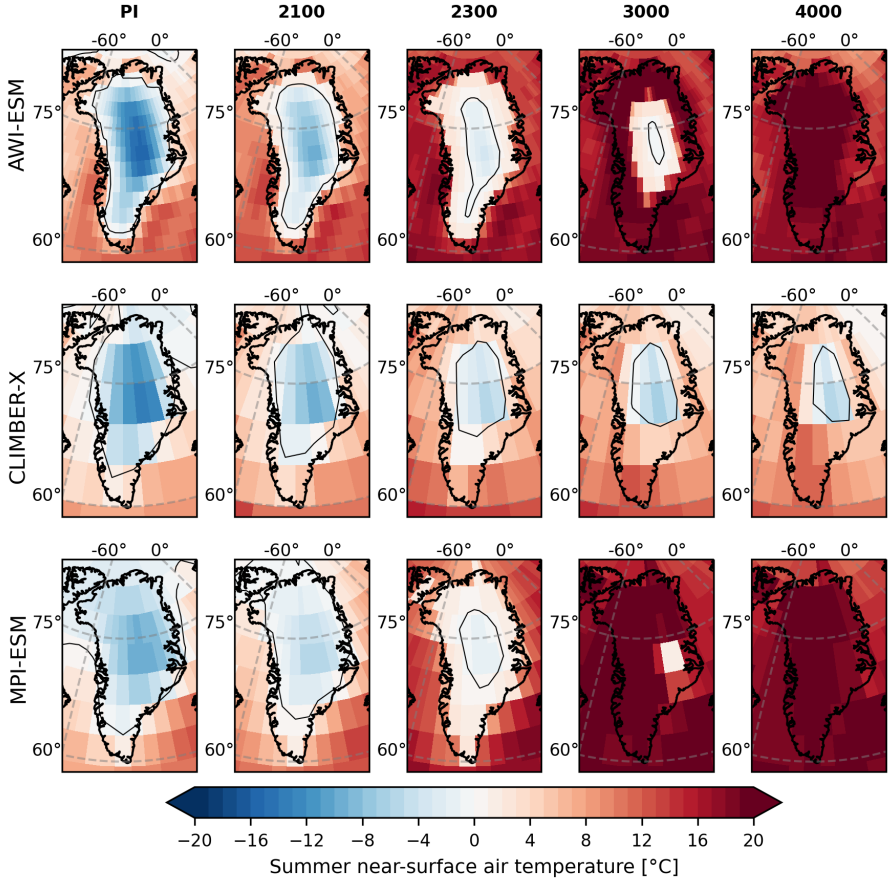

Figure A9. Similar to Fig. 5 but for SSP5-8.5.

https://doi.org/10.5194/egusphere-2026-3384
Preprint. Discussion started: 6 July 2026

	AWI-ESM	CLIMBER-X	MPI-ESM
Ice sheets			
Basal sliding law	pseudo-plastic power law	Weertmann-type	pseudo-plastic power law
Geothermal heatflux	Shapiro and Ritzwoller (2004)	55 mW/m^2	42 mW/m^2
Calving	Eigencalving and thickness threshold calving	Thickness threshold calving	Eigencalving and thickness threshold calving
Basal hydrology	none	none	Undrained plastic bed model
Ice flow law	Glen's flow law	Glen's flow law	Glen's flow law
Flow law exponent	3	3	3
GIA			
Included	No	Yes	Yes
Viscosity structure	–	3D (Bagge et al., 2021)	1D (Mikolajewicz et al., 2025)
Initial topography	BEDMAP (Bamber et al., 2001)	RTopo-2 (Schaffer et al., 2016)	RTopo-2 (Schaffer et al., 2016)

Table A1. Parameter table for ice sheet and solid Earth modelling components.

Scenario	Year	AWI-ESM	CLIMBER-X	MPI-ESM
SSP2-4.5	2100	0.06	0.03	0.06
	2300	0.27	0.11	0.19
	2500	0.47	0.18	0.34
	3000	0.87	0.27	0.69
	4000	1.57	0.38	1.52
SSP4-6.0	2100	0.08	0.03	0.07
	2300	0.39	0.19	0.32
	2500	0.75	0.38	0.64
	3000	1.54	0.73	1.66
	4000	2.81	1.36	4.23
SSP5-8.5	2100	0.09	0.04	0.11
	2300	0.99	0.57	1.34
	2500	2.36	1.30	3.50
	3000	5.27	2.76	7.17
	4000	7.31	4.33	7.29

Table A2. Volume changes of the GrIS relative to PI in m SLE for the three model systems and scenarios. Values are based on the periods defined in Section 2.

https://doi.org/10.5194/egusphere-2026-3384
Preprint. Discussion started: 6 July 2026

Model	Spin-up strategy	Spin-up length	Coupling frequency
CLIMBER-X	coupled pre-industrial equilibrium with climate-ice sheet model, followed by transient spin-up	pre-industrial: 50,000 years (asynchronous, climate accelerated by a factor of 5); transient: 1000–1849 CE (synchronous, no acceleration)	annual
AWI-ESM	separate spin-ups for climate model from equilibrium pre-industrial climate and ice sheet model from BEDMAP (Bamber et al., 2001), followed by a coupled pre-industrial spin-up	ice sheet (standalone): 50,000 years; climate model (standalone): 1,500 years; coupled climate-ice sheet: 600 years (asynchronous, factor 5); coupled climate-ice sheet: 130 years (synchronous)	annual
MPI-ESM	coupled pre-industrial equilibrium spin-up with climate-ice sheet model, followed by coupled transient spin-up	pre-industrial: 38,800 years, (asynchronous; factor 10); transient: 1100-1849 CE (synchronous)	annual

Table A3. Simulation setup for the three model systems, including the spin-up strategy, spin-up length and the coupling frequency between the climate and the ice-sheet models.

https://doi.org/10.5194/egusphere-2026-3384
Preprint. Discussion started: 6 July 2026

Code and data availability. All data required to reproduce the figures will be uploaded to the Zenodo database upon publication

Author contributions. CS, LA, MLK, MW and UM designed the study. MPI-ESM simulations were performed by MLK and UM, AWI-ESM simulations by LA and Climber-X simulations by MW. CS analysed the simulations and wrote the manuscript together with MLK and input from all co-authors.

Competing interests. At least one of the (co-)authors serves as editor for the special issue to which this paper belongs.

Acknowledgements. CS, LA, MLK, and MW were supported by the German Federal Ministry of Research, Technology and Space (BMFTR) as a Research for Sustainability initiative (FONA) through the PalMod project under grant numbers 01LP2302A, 01LP2313A, 01LP2316A, 01LP2305B. For all simulations, computing resources of the Deutsches Klimarechenzentrum (DKRZ) granted by its Scientific Steering Committee (WLA) under project ID ba0989 were used. MW gratefully acknowledges the European Regional Development Fund (ERDF) and the Land Brandenburg for supporting this project by providing resources on the high performance computer system at the Potsdam Institute for Climate Impact Research. We thank Hauke Schmidt for comments which improved an earlier version of the paper

https://doi.org/10.5194/egusphere-2026-3384
Preprint. Discussion started: 6 July 2026

References

Ackermann, L., Danek, C., Gierz, P., and Lohmann, G.: AMOC recovery in a multicentennial scenario using a coupled atmosphere-ocean-ice sheet model, Geophysical Research Letters, 47, e2019GL086 810, 2020.

Andernach, M., Kapsch, M.-L., and Mikolajewicz, U.: Stabilizing feedbacks allow for multiple states of the Greenland Ice Sheet in a fully coupled Earth System – Ice Sheet Model, The Cryosphere, 20, 1047–1069, https://doi.org/10.5194/tc-20-1047-2026, 2026.

Arakawa, A. and Lamb, V. R.: Computational Design of the Basic Dynamical Processes of the UCLA General Circulation Model, p. 173–265, Elsevier, ISBN 9780124608177, https://doi.org/10.1016/b978-0-12-460817-7.50009-4, 1977.

Arthern, R. J. and Gudmundsson, G. H.: Initialization of ice-sheet forecasts viewed as an inverse Robin problem, Journal of Glaciology, 56, 527–533, https://doi.org/10.3189/002214310792447699, 2010.

Aschwanden, A., Fahnestock, M. A., Truffer, M., Brinkerhoff, D. J., Hock, R., Khroulev, C., Mottram, R., and Khan, S. A.: Contribution of the Greenland Ice Sheet to sea level over the next millennium, Science Advances, 5, https://doi.org/10.1126/sciadv.aav9396, 2019.

Aschwanden, A., Bartholomaus, T. C., Brinkerhoff, D. J., and Truffer, M.: Brief communication: A roadmap towards credible projections of ice sheet contribution to sea level, The Cryosphere, 15, 5705–5715, https://doi.org/10.5194/tc-15-5705-2021, 2021.

Aðalgeirsdóttir, G., Aschwanden, A., Khroulev, C., Boberg, F., Mottram, R., Lucas-Picher, P., and Christensen, J.: Role of model initialization for projections of 21st-century Greenland ice sheet mass loss, Journal of Glaciology, 60, 782–794, https://doi.org/10.3189/2014jog13j202, 2014.

Bagge, M., Klemann, V., Steinberger, B., Latinović, M., and Thomas, M.: Glacial-Isostatic Adjustment Models Using Geodynamically Constrained 3D Earth Structures, Geochemistry, Geophysics, Geosystems, 22, 1–21, https://doi.org/10.1029/2021GC009853, 2021.

Bamber, J. L., Layberry, R. L., and Gogineni, S.: A new ice thickness and bed data set for the Greenland ice sheet: 1. Measurement, data reduction, and errors, Journal of Geophysical Research: Atmospheres, 106, 33 773–33 780, 2001.

Berger, A. and Loutre, M.: Insolation values for the climate of the last 10 million years, Quaternary Science Reviews, 10, 297–317, https://doi.org/10.1016/0277-3791(91)90033-q, 1991.

Calov, R. and Greve, R.: A semi-analytical solution for the positive degree-day model with stochastic temperature variations, Journal of Glaciology, 51, 173–175, 2005.

Calov, R., Ganopolski, A., Claussen, M., Petoukhov, V., and Greve, R.: Transient Simulation of the Last Glacial Inception. Part I: Glacial Inception as a Bifurcation in the Climate System, Climate Dynamics, 24, 545–561, https://doi.org/10.1007/s00382-005-0007-6, 2005.

Calov, R., Robinson, a., Perrette, M., and Ganopolski, a.: Simulating the Greenland ice sheet under present-day and palaeo constraints including a new discharge parameterization, The Cryosphere, 9, 179–196, https://doi.org/10.5194/tc-9-179-2015, 2015.

Calov, R., Beyer, S., Greve, R., Beckmann, J., Willeit, M., Kleiner, T., Rückamp, M., Humbert, A., and Ganopolski, A.: Simulation of the Future Sea Level Contribution of Greenland with a New Glacial System Model, Cryosphere, 12, 3097–3121, https://doi.org/10.5194/tc-12-3097-2018, 2018.

Danilov, S., Sidorenko, D., Wang, Q., and Jung, T.: The finite-volume sea ice–ocean model (FESOM2), Geoscientific Model Development, 10, 765–789, 2017.

Depsky, N., Bolliger, I., Allen, D., Choi, J. H., Delgado, M., Greenstone, M., Hamidi, A., Houser, T., Kopp, R. E., and Hsiang, S.: DSCIM-Coastal v1.1: an open-source modeling platform for global impacts of sea level rise, Geoscientific Model Development, 16, 4331–4366, https://doi.org/10.5194/gmd-16-4331-2023, 2023.

https://doi.org/10.5194/egusphere-2026-3384
Preprint. Discussion started: 6 July 2026

Edwards, N. R. and Marsh, R.: Uncertainties due to transport-parameter sensitivity in an efficient 3-D ocean-climate model, Climate Dynamics, 24, 415–433, https://doi.org/10.1007/s00382-004-0508-8, 2005.

Edwards, N. R., Willmott, A. J., and Killworth, P. D.: On the Role of Topography and Wind Stress on the Stability of the Thermohaline Circulation, Journal of Physical Oceanography, 28, 756–778, https://doi.org/10.1175/1520-0485(1998)028<0756:OTROTA>2.0.CO;2, 1998.

Erokhina, O. and Mikolajewicz, U.: A New Eulerian Iceberg Module for Climate Studies, Journal of Advances in Modeling Earth Systems, 16, https://doi.org/10.1029/2023ms003807, 2024.

Fettweis, X., Hofer, S., Krebs-Kanzow, U., Amory, C., Aoki, T., Berends, C. J., Born, A., Box, J. E., Delhasse, A., Fujita, K., Gierz, P., Goelzer, H., Hanna, E., Hashimoto, A., Huybrechts, P., Kapsch, M.-L., King, M. D., Kittel, C., Lang, C., Langen, P. L., Lenaerts, J. T. M., Liston, G. E., Lohmann, G., Mernild, S. H., Mikolajewicz, U., Modali, K., Mottram, R. H., Niwano, M., Noël, B., Ryan, J. C., Smith, A., Streffing, J., Tedesco, M., van de Berg, W. J., van den Broeke, M., van de Wal, R. S. W., van Kampenhout, L., Wilton, D., Wouters, B., Ziemen, F., and Zolles, T.: GrSMBMIP: intercomparison of the modelled 1980–2012 surface mass balance over the Greenland Ice Sheet, The Cryosphere, 14, 3935–3958, https://doi.org/10.5194/tc-14-3935-2020, 2020.

Fürst, J. J., Goelzer, H., and Huybrechts, P.: Ice-dynamic projections of the Greenland ice sheet in response to atmospheric and oceanic warming, The Cryosphere, 9, 1039–1062, https://doi.org/10.5194/tc-9-1039-2015, 2015.

Fyke, J. G., Vizcaíno, M., and Lipscomb, W. H.: The pattern of anthropogenic signal emergence in Greenland Ice Sheet surface mass balance, Geophysical Research Letters, 41, 6002–6008, https://doi.org/10.1002/2014gl060735, 2014.

Ganopolski, A., Calov, R., and Claussen, M.: Simulation of the last glacial cycle with a coupled climate ice-sheet model of intermediate complexity, Climate of the Past, 6, 229–244, https://doi.org/10.5194/cp-6-229-2010, 2010.

Goelzer, H., Nowicki, S., Edwards, T., Beckley, M., Abe-Ouchi, A., Aschwanden, A., Calov, R., Gagliardini, O., Gillet-Chaulet, F., Golledge, N. R., Gregory, J., Greve, R., Humbert, A., Huybrechts, P., Kennedy, J. H., Larour, E., Lipscomb, W. H., Le clec'h, S., Lee, V., Morlighem, M., Pattyn, F., Payne, A. J., Rodehacke, C., Rückamp, M., Saito, F., Schlegel, N., Seroussi, H., Shepherd, A., Sun, S., van de Wal, R., and Ziemen, F. A.: Design and results of the ice sheet model initialisation experiments initMIP-Greenland: an ISMIP6 intercomparison, The Cryosphere, 12, 1433–1460, https://doi.org/10.5194/tc-12-1433-2018, 2018.

Goelzer, H., Nowicki, S., Payne, A., Larour, E., Seroussi, H., Lipscomb, W. H., Gregory, J., Abe-Ouchi, A., Shepherd, A., Simon, E., Agosta, C., Alexander, P., Aschwanden, A., Barthel, A., Calov, R., Chambers, C., Choi, Y., Cuzzone, J., Dumas, C., Edwards, T., Felikson, D., Fettweis, X., Golledge, N. R., Greve, R., Humbert, A., Huybrechts, P., Le clec'h, S., Lee, V., Leguy, G., Little, C., Lowry, D. P., Morlighem, M., Nias, I., Quiquet, A., Rückamp, M., Schlegel, N.-J., Slater, D. A., Smith, R. S., Straneo, F., Tarasov, L., van de Wal, R., and van den Broeke, M.: The future sea-level contribution of the Greenland ice sheet: a multi-model ensemble study of ISMIP6, The Cryosphere, 14, 3071–3096, https://doi.org/10.5194/tc-14-3071-2020, 2020.

Goelzer, H., Langebroek, P. M., Born, A., Hofer, S., Haubner, K., Petrini, M., Leguy, G., Lipscomb, W. H., and Thayer-Calder, K.: Interactive coupling of a Greenland ice sheet model in NorESM2, Geoscientific Model Development, 18, 7853–7867, https://doi.org/10.5194/gmd-18-7853-2025, 2025.

Gregory, J. M., Ingram, W. J., Palmer, M. A., Jones, G. S., Stott, P. A., Thorpe, R. B., Lowe, J. A., Johns, T. C., and Williams, K. D.: A new method for diagnosing radiative forcing and climate sensitivity, Geophysical Research Letters, 31, https://doi.org/10.1029/2003gl018747, 2004.

Greve, R.: Application of a Polythermal Three-Dimensional Ice Sheet Model to the Greenland Ice Sheet: Response to Steady-State and Transient Climate Scenarios, Journal of Climate, 10, 901–918, https://doi.org/10.1175/1520-0442(1997)010<0901:AOAPTD>2.0.CO;2, 1997.

https://doi.org/10.5194/egusphere-2026-3384
Preprint. Discussion started: 6 July 2026

Hagemann, S. and Dümenil, L.: A parametrization of the lateral waterflow for the global scale, Climate dynamics, 14, 17–31, 1997.

Haubner, K., Goelzer, H., and Born, A.: Limited global effect of climate-Greenland ice sheet coupling in NorESM2 under a high-emission scenario, Earth System Dynamics, 17, 57–80, https://doi.org/10.5194/esd-17-57-2026, 2026.

Hofer, S., Lang, C., Amory, C., Kittel, C., Delhasse, A., Tedstone, A., and Fettweis, X.: Greater Greenland Ice Sheet contribution to global sea level rise in CMIP6, Nature Communications, 11, https://doi.org/10.1038/s41467-020-20011-8, 2020.

Ilyina, T., Six, K. D., Segschneider, J., Maier-Reimer, E., Li, H., and Núñez-Riboni, I.: Global ocean biogeochemistry model HAMOCC: Model architecture and performance as component of the MPI-Earth system model in different CMIP5 experimental realizations, Journal of Advances in Modeling Earth Systems, 5, 287–315, https://doi.org/10.1029/2012MS000178, 2013.

Kageyama, M., Harrison, S. P., Kapsch, M.-L., Lofverstrom, M., Lora, J. M., Mikolajewicz, U., Sherriff-Tadano, S., Vadsaria, T., Abe-Ouchi, A., Bouttes, N., Chandan, D., Gregoire, L. J., Ivanovic, R. F., Izumi, K., LeGrande, A. N., Lhardy, F., Lohmann, G., Morozova, P. A., Ohgaito, R., Paul, A., Peltier, W. R., Poulsen, C. J., Quiquet, A., Roche, D. M., Shi, X., Tierney, J. E., Valdes, P. J., Volodin, E., and Zhu, J.: The PMIP4 Last Glacial Maximum experiments: preliminary results and comparison with the PMIP3 simulations, Climate of the Past, 17, 1065–1089, https://doi.org/10.5194/cp-17-1065-2021, 2021.

Kapsch, M.-L., Mikolajewicz, U., Ziemen, F. A., Rodehacke, C. B., and Schannwell, C.: Analysis of the surface mass balance for deglacial climate simulations, The Cryosphere, 15, 1131–1156, https://doi.org/10.5194/tc-15-1131-2021, 2021.

Kaufhold, C., Willeit, M., Talento, S., Ganopolski, A., and Rockström, J.: Interplay between climate and carbon cycle feedbacks could substantially enhance future warming, Environmental Research Letters, 20, 044 027, https://doi.org/10.1088/1748-9326/adb6be, 2025.

Kirezci, E., Young, I. R., Ranasinghe, R., Muis, S., Nicholls, R. J., Lincke, D., and Hinkel, J.: Projections of global-scale extreme sea levels and resulting episodic coastal flooding over the 21st Century, Scientific Reports, 10, https://doi.org/10.1038/s41598-020-67736-6, 2020.

Klemann, V., Martinec, Z., and Ivins, E. R.: Glacial isostasy and plate motion, Journal of Geodynamics, 46, 95–103, https://doi.org/10.1016/j.jog.2008.04.005, 2008.

Krebs-Kanzow, U., Gierz, P., Rodehacke, C. B., Xu, S., Yang, H., and Lohmann, G.: The diurnal Energy Balance Model (dEBM): a convenient surface mass balance solution for ice sheets in Earth system modeling, The Cryosphere, 15, 2295–2313, 2021.

Laskar, J., Robutel, P., Joutel, F., Gastineau, M., Correia, A. C. M., and Levrard, B.: A long-term numerical solution for the insolation quantities of the Earth, Astronomy amp; Astrophysics, 428, 261–285, https://doi.org/10.1051/0004-6361:20041335, 2004.

Madsen, M. S., Yang, S., Aðalgeirsdóttir, G., Svendsen, S. H., Rodehacke, C. B., and Ringgaard, I. M.: The role of an interactive Greenland ice sheet in the coupled climate-ice sheet model EC-Earth-PISM, Climate Dynamics, 59, 1189–1211, https://doi.org/10.1007/s00382-022-06184-6, 2022.

Mankoff, K. D., Fettweis, X., Langen, P. L., Stendel, M., Kjeldsen, K. K., Karlsson, N. B., Noël, B., van den Broeke, M. R., Solgaard, A., Colgan, W., Box, J. E., Simonsen, S. B., King, M. D., Ahlstrøm, A. P., Andersen, S. B., and Fausto, R. S.: Greenland ice sheet mass balance from 1840 through next week, Earth System Science Data, 13, 5001–5025, https://doi.org/10.5194/essd-13-5001-2021, 2021.

Marsland, S., Haak, H., Jungclaus, J., Latif, M., and Röske, F.: The Max-Planck-Institute global ocean/sea ice model with orthogonal curvilinear coordinates, Ocean Modelling, 5, 91 – 127, https://doi.org/https://doi.org/10.1016/S1463-5003(02)00015-X, 2003.

Martin, M., Winkelmann, R., Haseloff, M., Albrecht, T., Bueler, E., Khroulev, C., and Levermann, A.: The Potsdam parallel ice sheet model (PISM-PIK)–Part 2: dynamic equilibrium simulation of the Antarctic ice sheet, The Cryosphere, 5, 727–740, 2011.

Martinec, Z., Klemann, V., van der Wal, W., Riva, R. E., Spada, G., Sun, Y., Melini, D., Kachuck, S. B., Barletta, V., Simon, K., A, G., and James, T. S.: A benchmark study of numerical implementations of the sea level equation in GIA modelling, Geophysical Journal International, 215, 389–414, https://doi.org/10.1093/gji/ggy280, 2018.

https://doi.org/10.5194/egusphere-2026-3384
Preprint. Discussion started: 6 July 2026

Mauritsen, T., Bader, J., Becker, T., Behrens, J., Bittner, M., Brokopf, R., Brovkin, V., Claussen, M., Crueger, T., Esch, M., Fast, I., Fiedler, S., Fläschner, D., Gayler, V., Giorgetta, M., Goll, D. S., Haak, H., Hagemann, S., Hedemann, C., Hohenegger, C., Ilyina, T., Jahns, T., Jimenéz-de-la Cuesta, D., Jungclaus, J., Kleinen, T., Kloster, S., Kracher, D., Kinne, S., Kleberg, D., Lasslop, G., Kornblueh, L., Marotzke, J., Matei, D., Meraner, K., Mikolajewicz, U., Modali, K., Möbis, B., Müller, W. A., Nabel, J. E., Nam, C. C., Notz, D., Nyawira, S. S., Paulsen, H., Peters, K., Pincus, R., Pohlmann, H., Pongratz, J., Popp, M., Raddatz, T. J., Rast, S., Redler, R., Reick, C. H., Rohrschneider, T., Schemann, V., Schmidt, H., Schnur, R., Schulzweida, U., Six, K. D., Stein, L., Stemmler, I., Stevens, B., von Storch, J. S., Tian, F., Voigt, A., Vrese, P., Wieners, K. H., Wilkenskjeld, S., Winkler, A., and Roeckner, E.: Developments in the MPI-M Earth System Model version 1.2 (MPI-ESM1.2) and Its Response to Increasing CO_2, Journal of Advances in Modeling Earth Systems, 11, 998–1038, https://doi.org/10.1029/2018MS001400, 2019.

Meccia, V. L. and Mikolajewicz, U.: Interactive ocean bathymetry and coastlines for simulating the last deglaciation with the Max Planck Institute Earth System Model (MPI-ESM-v1.2), Geoscientific Model Development, 11, 4677–4692, https://doi.org/10.5194/gmd-11-4677-2018, 2018.

Mikolajewicz, U., Gröger, M., Maier-Reimer, E., Schurgers, G., Vizcaíno, M., and Winguth, A. M. E.: Long-term effects of anthropogenic CO2 emissions simulated with a complex earth system model, Climate Dynamics, 28, 599–633, https://doi.org/10.1007/s00382-006-0204-y, 2007a.

Mikolajewicz, U., Vizcaíno, M., Jungclaus, J., and Schurgers, G.: Effect of ice sheet interactions in anthropogenic climate change simulations, Geophysical Research Letters, 34, https://doi.org/10.1029/2007gl031173, 2007b.

Mikolajewicz, U., Kapsch, M.-L., Schannwell, C., Six, K. D., Ziemen, F. A., Bagge, M., Baudouin, J.-P., Erokhina, O., Gayler, V., Klemann, V., Meccia, V. L., Mouchet, A., and Riddick, T.: Deglaciation and abrupt events in a coupled comprehensive atmosphere–ocean–ice-sheet–solid-earth model, Climate of the Past, 21, 719–751, https://doi.org/10.5194/cp-21-719-2025, 2025.

Morlighem, M., Williams, C. N., Rignot, E., An, L., Arndt, J. E., Bamber, J. L., Catania, G., Chauché, N., Dowdeswell, J. A., Dorschel, B., Fenty, I., Hogan, K., Howat, I., Hubbard, A., Jakobsson, M., Jordan, T. M., Kjeldsen, K. K., Millan, R., Mayer, L., Mouginot, J., Noël, B. P. Y., O'Cofaigh, C., Palmer, S., Rysgaard, S., Seroussi, H., Siegert, M. J., Slabon, P., Straneo, F., van den Broeke, M. R., Weinrebe, W., Wood, M., and Zinglersen, K. B.: BedMachine v3: Complete Bed Topography and Ocean Bathymetry Mapping of Greenland From Multibeam Echo Sounding Combined With Mass Conservation, Geophysical Research Letters, 44, https://doi.org/10.1002/2017gl074954, 2017.

Muntjewerf, L., Sellevold, R., Vizcaino, M., Ernani da Silva, C., Petrini, M., Thayer-Calder, K., Scherrenberg, M. D. W., Bradley, S. L., Katsman, C. A., Fyke, J., Lipscomb, W. H., Lofverstrom, M., and Sacks, W. J.: Accelerated Greenland Ice Sheet Mass Loss Under High Greenhouse Gas Forcing as Simulated by the Coupled CESM2.1-CISM2.1, Journal of Advances in Modeling Earth Systems, 12, https://doi.org/10.1029/2019ms002031, 2020.

Niu, L., Knorr, G., Krebs-Kanzow, U., Gierz, P., and Lohmann, G.: Rapid Laurentide Ice Sheet growth preceding the Last Glacial Maximum due to summer snowfall, Nature Geoscience, 17, 440–449, 2024.

Niu, L., Knorr, G., Ackermann, L., Krebs-Kanzow, U., and Lohmann, G.: Eurasian ice sheet formation promoted by weak AMOC following MIS 3, npj Climate and Atmospheric Science, 8, 85, 2025.

Oerlemans, J. and Knap, W. H.: A 1 year record of global radiation and albedo in the ablation zone of Morteratschgletscher, Switzerland, Journal of Glaciology, 44, 231–238, https://doi.org/10.3189/s0022143000002574, 1998.

Paice, C. M., Fettweis, X., and Huybrechts, P.: Positive feedbacks drive the Greenland ice sheet evolution in millennial-length MAR–GISM simulations under a high-end warming scenario, The Cryosphere, 20, 309–332, https://doi.org/10.5194/tc-20-309-2026, 2026.

https://doi.org/10.5194/egusphere-2026-3384
Preprint. Discussion started: 6 July 2026

Raddatz, T. J., Reick, C. H., Knorr, W., Kattge, J., Roeckner, E., Schnur, R., Schnitzler, K. G., Wetzel, P., and Jungclaus, J.: Will the tropical land biosphere dominate the climate–carbon cycle feedback during the twenty-first century?, Climate Dynamics, 29, 565–574, https://doi.org/10.1007/s00382-007-0247-8, 2007.

Rahlves, C., Goelzer, H., Born, A., and Langebroek, P. M.: Historically consistent mass loss projections of the Greenland ice sheet, The Cryosphere, 19, 1205–1220, https://doi.org/10.5194/tc-19-1205-2025, 2025.

Reick, C. H., Gayler, V., Goll, D., Hagemann, S., Heidkamp, M., Nabel, J. E., Raddatz, T., Roeckner, E., Schnur, R., and Wilkenskjeld, S.: JSBACH 3-The land component of the MPI Earth System Model: documentation of version 3.2, 2021.

Renoult, M., Annan, J. D., Hargreaves, J. C., Sagoo, N., Flynn, C., Kapsch, M.-L., Li, Q., Lohmann, G., Mikolajewicz, U., Ohgaito, R., Shi, X., Zhang, Q., and Mauritsen, T.: A Bayesian framework for emergent constraints: case studies of climate sensitivity with PMIP, Climate of the Past, 16, 1715–1735, https://doi.org/10.5194/cp-16-1715-2020, 2020.

Riddick, T., Brovkin, V., Hagemann, S., and Mikolajewicz, U.: Dynamic hydrological discharge modelling for coupled climate model simulations of the last glacial cycle: the MPI-DynamicHD model version 3.0, Geoscientific Model Development, 11, 4291–4316, https://doi.org/10.5194/gmd-11-4291-2018, 2018.

Ridley, J. K., Huybrechts, P., Gregory, J. M., and Lowe, J. A.: Elimination of the Greenland Ice Sheet in a High CO2 Climate, Journal of Climate, 18, 3409–3427, https://doi.org/10.1175/jcli3482.1, 2005.

Schaffer, J., Timmermann, R., Arndt, J. E., Kristensen, S. S., Mayer, C., Morlighem, M., and Steinhage, D.: A global, high-resolution data set of ice sheet topography, cavity geometry, and ocean bathymetry, Earth System Science Data, 8, 543–557, https://doi.org/10.5194/essd-8-543-2016, 2016.

Sein, D. V., Danilov, S., Biastoch, A., Durgadoo, J. V., Sidorenko, D., Harig, S., and Wang, Q.: Designing variable ocean model resolution based on the observed ocean variability, Journal of Advances in Modeling Earth Systems, 8, 904–916, 2016.

Seroussi, H., Nowicki, S., Payne, A. J., Goelzer, H., Lipscomb, W. H., Abe-Ouchi, A., Agosta, C., Albrecht, T., Asay-Davis, X., Barthel, A., Calov, R., Cullather, R., Dumas, C., Galton-Fenzi, B. K., Gladstone, R., Golledge, N. R., Gregory, J. M., Greve, R., Hattermann, T., Hoffman, M. J., Humbert, A., Huybrechts, P., Jourdain, N. C., Kleiner, T., Larour, E., Leguy, G. R., Lowry, D. P., Little, C. M., Morlighem, M., Pattyn, F., Pelle, T., Price, S. F., Quiquet, A., Reese, R., Schlegel, N.-J., Shepherd, A., Simon, E., Smith, R. S., Straneo, F., Sun, S., Trusel, L. D., Van Breedam, J., van de Wal, R. S. W., Winkelmann, R., Zhao, C., Zhang, T., and Zwinger, T.: ISMIP6 Antarctica: a multi-model ensemble of the Antarctic ice sheet evolution over the 21st century, The Cryosphere, 14, 3033–3070, https://doi.org/10.5194/tc-14-3033-2020, 2020.

Shapiro, N. M. and Ritzwoller, M. H.: Inferring surface heat flux distributions guided by a global seismic model: particular application to Antarctica, Earth and Planetary Science Letters, 223, 213–224, https://doi.org/https://doi.org/10.1016/j.epsl.2004.04.011, 2004.

Stevens, B., Giorgetta, M., Esch, M., Mauritsen, T., Crueger, T., Rast, S., Salzmann, M., Schmidt, H., Bader, J., Block, K., Brokopf, R., Fast, I., Kinne, S., Kornblueh, L., Lohmann, U., Pincus, R., Reichler, T., and Roeckner, E.: Atmospheric component of the MPI-M Earth System Model: ECHAM6, Journal of Advances in Modeling Earth Systems, 5, 146–172, https://doi.org/10.1002/jame.20015, 2013.

Vizcaino, M., Mikolajewicz, U., Ziemen, F., Rodehacke, C. B., Greve, R., and van den Broeke, M. R.: Coupled simulations of Greenland Ice Sheet and climate change up to A.D. 2300, Geophysical Research Letters, 42, 3927–3935, https://doi.org/10.1002/2014gl061142, 2015.

Vizcaíno, M., Mikolajewicz, U., Gröger, M., Maier-Reimer, E., Schurgers, G., and Winguth, A. M. E.: Long-term ice sheet–climate interactions under anthropogenic greenhouse forcing simulated with a complex Earth System Model, Climate Dynamics, 31, 665–690, https://doi.org/10.1007/s00382-008-0369-7, 2008.

https://doi.org/10.5194/egusphere-2026-3384
Preprint. Discussion started: 6 July 2026

Willeit, M. and Ganopolski, A.: PALADYN v1.0, a comprehensive land surface–vegetation–carbon cycle model of intermediate complexity, Geoscientific Model Development, 9, 3817–3857, https://doi.org/10.5194/gmd-9-3817-2016, 2016.

Willeit, M., Ganopolski, A., Robinson, A., and Edwards, N. R.: The Earth system model CLIMBER-X v1.0 – Part 1: Climate model description and validation, Geoscientific Model Development, 15, 5905–5948, https://doi.org/10.5194/gmd-15-5905-2022, 2022.

Willeit, M., Ilyina, T., Liu, B., Heinze, C., Perrette, M., Heinemann, M., Dalmonech, D., Brovkin, V., Munhoven, G., Börker, J., Hartmann, J., Romero-Mujalli, G., and Ganopolski, A.: The Earth system model CLIMBER-X v1.0 – Part 2: The global carbon cycle, Geoscientific Model Development, 16, 3501–3534, https://doi.org/10.5194/gmd-16-3501-2023, 2023.

Willeit, M., Calov, R., Talento, S., Greve, R., Bernales, J., Klemann, V., Bagge, M., and Ganopolski, A.: Glacial inception through rapid ice area increase driven by albedo and vegetation feedbacks, Climate of the Past, 20, 597–623, https://doi.org/10.5194/cp-20-597-2024, 2024.

Winkelmann, R., Martin, M. A., Haseloff, M., Albrecht, T., Bueler, E., Khroulev, C., and Levermann, A.: The Potsdam parallel ice sheet model (PISM-PIK)–Part 1: Model description, The Cryosphere, 5, 715–726, 2011.

Ziemen, F. A., Kapsch, M.-L., Klockmann, M., and Mikolajewicz, U.: Heinrich events show two-stage climate response in transient glacial simulations, Climate of the Past, 15, 153–168, https://doi.org/10.5194/cp-15-153-2019, 2019.